Research on Engineering Structures & Materials
www.jresm.org
MIM Research Group

Research Article

Enhancing the seismic performance of plan irregular L-shaped reinforced concrete buildings using steel bracing systems

Hossein Jarrahi [1,a], Abbasali Sadeghi [*,2,b], S. Javad Vaziri [3,c]

[1]*Department of Civil Engineering, University of Birjand, Birjand, Iran*
[2]*Department of Civil Engineering, Ma.C., Islamic Azad University, Mashhad, Iran*
[3]*Department of Civil Engineering, Semnan University, Semnan, Iran*

Article Info

Article History:

Received 26 May 2026

Accepted 02 Sep 2026

Keywords:

Performance levels; Reinforced concrete (RC) structure; Steel bracing; Plan irregularity; Nonlinear analysis

Abstract

Seismic retrofitting of existing reinforced concrete (RC) buildings is often required because of deficiencies in their original design, changes in seismic provisions, or increased functional demands. This study evaluates the effectiveness of steel bracing for improving the seismic performance of a ten-story, plan-irregular, L-shaped RC building. Nonlinear static pushover analyses and nonlinear dynamic analyses were performed for both the unretrofitted and retrofitted models. The response was evaluated in terms of plastic-hinge development, structural performance level, displacement demand, and base-shear capacity. The dynamic analyses were conducted using the Tabas, Northridge, and Landers ground motions after applying the specified record-processing and orthogonal-component procedures. The results indicate that the addition of steel bracing improves the seismic behavior of the investigated structure by increasing its lateral resistance and reducing its displacement demand. Based on the reported pushover results, the maximum displacement decreased from 0.4176 m to 0.0677 m, corresponding to a reduction of 83.8%, while the maximum base shear increased from 472.669 kN to 593.901 kN, corresponding to an increase of 25.6%. In addition, the results show that more than 80% of the columns remained undamaged after strengthening. These findings suggest that steel bracing can be an effective retrofit strategy for the investigated L-shaped RC building. However, because the study is based on a single numerical case study, the findings should not be generalized to all plan-irregular reinforced-concrete buildings without further parametric and experimental investigations.

1. Introduction

Since the earliest stages of human civilization, natural hazards have posed significant challenges to societies, necessitating continuous efforts to mitigate their impacts and enhance the resilience of the built environment. Among these hazards, earthquakes are recognized as one of the most destructive, owing to their sudden occurrence and potentially catastrophic consequences. Evidence from past seismic events, combined with the observed deficiencies in a considerable portion of existing building stocks. Numerous vulnerability assessments have further confirmed that a substantial number of existing structures are highly susceptible to damage or collapse under strong ground motions [1]. Given that earthquakes cannot be prevented, improving the seismic performance of existing structures through retrofitting becomes an essential and inevitable strategy. Seismic retrofitting can be broadly defined as the systematic modification of an existing structure to enhance its strength, stiffness, and ductility, thereby enabling it to satisfy the required performance objectives under future seismic loading. In this context, the selection of an

*Corresponding author: abbasali.sadeghi@iau.ir
[a]orcid.org/0009-0004-2133-8470; [b]orcid.org/0000-0002-3016-9080; [c]orcid.org/0009-0005-5116-8297
DOI: http://dx.doi.org/10.17515/resm2026-1710st0526rs

appropriate retrofitting technique plays a critical role in achieving the desired structural performance while maintaining economic feasibility and constructability [2]. Among the various strengthening methods, the application of steel bracing systems has attracted considerable attention as an efficient solution for upgrading reinforced concrete (RC) frame structures. This method is not only relatively simple and cost-effective but also offers several practical advantages, including minimal additional mass, compatibility with existing structural configurations, and the possibility of preserving architectural functionality by allowing openings within the frame. The incorporation of steel braces enhances lateral stiffness and strength, reduces structural deformations, and improves overall energy dissipation capacity, leading to a more favorable seismic response [3, 4]. Although numerous studies have addressed the seismic strengthening of RC frame structures, most have primarily focused on regular configurations or single influencing parameters. In contrast, the present study aims to provide a more comprehensive evaluation by simultaneously considering two critical factors: building height and plan irregularity. Specifically, the seismic performance of a relatively tall, plan-irregular structure is assessed before and after retrofitting, with particular emphasis on performance levels and nonlinear behavior. A review of selected related studies in this field is presented in the following section.

2. Literature Review

Lateral load-resisting systems, including shear walls, moment-resisting frames, and braced systems, play a fundamental role in ensuring the seismic safety of structures by enhancing stiffness, strength, and energy dissipation capacity. Among these, steel bracing systems have increasingly been adopted not only in steel structures but also as an efficient retrofitting solution for deficient RC frame structures. This trend is primarily driven by their ease of implementation, cost-effectiveness, minimal additional mass, and reduced architectural interference compared to conventional strengthening techniques. A considerable body of research has focused on the seismic response of plan-irregular structures, particularly those with L-shaped configurations. It is well established that such irregularities lead to torsional amplification and stress concentration, thereby increasing structural vulnerability. For example, Khanal and Chaulagain [5] demonstrated that L-shaped buildings exhibit significantly higher sensitivity to the angle of seismic excitation, resulting in increased displacement, drift, and torsional irregularity. Similarly, Abdel Raheem et al. [6] reported that re-entrant corners in L-shaped buildings intensify lateral–torsional coupling effects, leading to higher seismic demands compared to regular configurations. In addition, Mazza [7] highlighted the importance of nonlinear analysis in identifying critical directions of seismic vulnerability in asymmetric RC buildings, emphasizing that plan irregularity significantly influences both strength and displacement capacities. Furthermore, recent studies have explored the seismic behavior of irregular steel and composite systems incorporating bracing mechanisms. Vaziri et al. [8] investigated L-shaped steel structures with BRBF systems and showed that soil–structure interaction (SSI) plays a crucial role in modifying seismic demands, particularly in terms of base shear and torsional response. In a complementary study, Vaziri et al. [9] examined the correlation between ground motion parameters and structural damage in L-shaped Buckling Restrained Braced Frame (BRBF) systems, concluding that spectral acceleration is a key indicator of damage, especially in low- and mid-rise structures. Moreover, the influence of ground motion characteristics was further examined by Vaziri et al. [10], who reported that near-fault pulse-like excitations impose significantly higher drift and acceleration demands compared to non-pulse-like motions. In addition to performance assessment, several researchers have focused on innovative design methodologies for improving seismic behavior. Jaberi et al. [11] proposed a collapse-based design (CBD) framework for irregular BRBF systems and demonstrated that it can accurately predict seismic performance while significantly reducing computational effort. Meanwhile, optimization-based approaches have been widely explored for enhancing structural resilience. For instance, Jarrahi et al. [12] developed a hybrid optimization framework for rotational friction dampers (RFDs), showing that optimal damper placement significantly improves energy dissipation and reduces inter-story drift. Similarly, other studies [13–15] emphasized the importance of optimizing damper parameters and configurations, revealing that a substantial portion of seismic input energy can be effectively dissipated through properly designed RFD systems, thereby reducing structural damage.

On the other hand, numerous studies have examined the effectiveness of different bracing configurations in improving the seismic performance of structures. Vaziri et al. [1] conducted a comprehensive numerical study on various bracing arrangements and concluded that X-bracing systems provide the highest stiffness and lowest displacement compared to other configurations. Similarly, Maheri and Fathi [16] showed that the configuration of X-bracing significantly influences load distribution and overall structural performance, with diagonally distributed arrangements yielding the most favorable results. Furthermore, Rahimi and Maheri [17] reported that while steel X-bracing improves global seismic response, its effectiveness decreases with increasing building height and may introduce local adverse effects in certain structural elements. Experimental and analytical investigations have also confirmed the beneficial effects of steel bracing systems. Kheyroddin et al. [18] experimentally demonstrated that steel bracing significantly enhances stiffness, strength, and energy dissipation capacity of RC frames, although different configurations may influence ductility performance. Similarly, Tan et al. [19] showed that steel X-bracing improves hysteretic behavior and promotes a more desirable global failure mechanism in RC space frames. Additionally, Ahiwale et al. [20] compared various bracing systems and concluded that the inclusion of steel braces substantially reduces drift and improves overall seismic resilience. In parallel, several studies have addressed the influence of connection details and bracing types on structural performance. Hodaipour and Ferdousi [21] highlighted the critical role of connection systems in determining stiffness, ductility, and energy dissipation capacity of braced RC frames. Likewise, Khan et al. [22] demonstrated that eccentric steel bracing systems significantly enhance lateral stiffness and reduce drift demands by altering load transfer mechanisms. Furthermore, alternative retrofitting techniques based on hysteretic damped braces and displacement-based design approaches have been explored. Mazza [23, 24] proposed advanced methodologies for retrofitting irregular RC structures using hysteretic damped braces, demonstrating their effectiveness in controlling torsional effects and improving seismic performance. Similarly, Ferraioli et al. [25] presented a practical case study of seismic retrofitting using dissipative steel braces, confirming the reliability of such systems through nonlinear analyses. Additionally, the influence of structural systems and configurations on seismic performance has been examined from broader perspectives. Saberi et al. [26] conducted seven scenarios in three states such as regular, very soft irregularity, and irregularity of cutting the lateral bearing system for 5-story model. The studied frames are evaluated by analyses of the equivalent static, spectral dynamics and time history dynamic. The results showed that time history dynamic analysis is more accurate than other methods. For example, the error rate of the maximum displacement response of frame with irregularity of cutting the lateral bearing system in equivalent static analysis compared to spectral and time history dynamic analyses are 15% and 77%, respectively. Poudel and Gyawali [27] investigated the role of slab systems in irregular buildings and found that optimized configurations can significantly enhance seismic behavior. Moreover, Chonratana and Chatpattananan [28] introduced a damage index approach for assessing seismic performance, emphasizing the importance of combining deformation and energy-based criteria in evaluating structural damage.

Despite the extensive research conducted in this field, most previous studies have focused on either regular structures, specific retrofitting techniques, or isolated parameters. However, the combined effects of plan irregularity, building height, and retrofitting strategies, particularly in RC frame structures retrofitted with steel bracing, have not been sufficiently addressed. Therefore, the present study aims to fill this gap by evaluating the seismic performance of a relatively tall, plan-irregular RC building before and after retrofitting using steel bracing systems. Through comprehensive nonlinear analyses, the study seeks to provide deeper insights into the effectiveness of this retrofitting approach in improving structural performance under seismic loading. Overall, the contribution of this study lies in examining the combined effects of building height, L-shaped plan irregularity, and steel bracing in a three-dimensional RC building using both nonlinear static and nonlinear dynamic analyses.

3. Model Description

In this section, the selected structural model is first introduced in detail. Subsequently, following the completion of the analysis and design procedures, the seismic performance level of the original (un-retrofitted) structure is evaluated. The plan configuration of the building is illustrated in Figure

1. All bays have a uniform span length of 5 m, and the story height is considered to be 3.2 m throughout the structure. Due to the presence of plan irregularity, the seismic response of the structure must be assessed by simultaneously accounting for the effects of bidirectional loading. Accordingly, nonlinear analyses are performed by considering 100% of the seismic demand in the principal direction under investigation, combined with 30% of the corresponding response in the orthogonal direction.

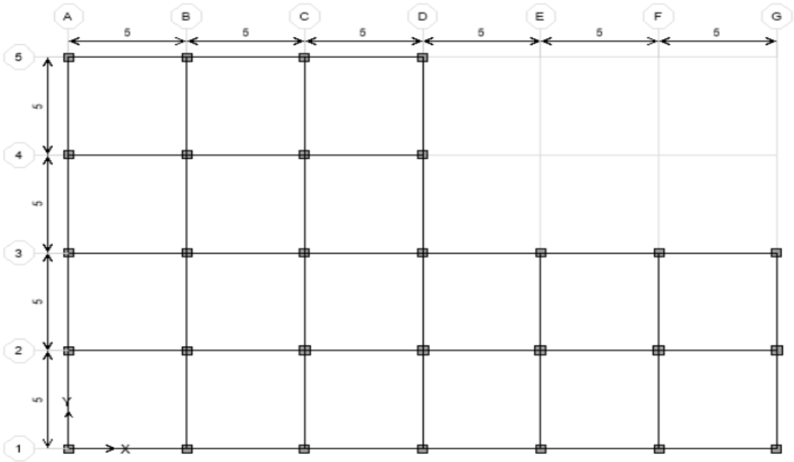

Fig. 1. Plan of the un-retrofitted model

This approach is consistent with widely accepted seismic design provisions for irregular structures [29, 30], where interaction between the two horizontal components of ground motion cannot be neglected. In practical terms, by applying the coefficients of 1.0 and 0.30, as specified in Table 1, the structure is subjected to full target displacement in one direction while simultaneously experiencing 30% of the target displacement in the perpendicular direction. This combined loading condition enables a more realistic representation of the structural behavior under multidirectional seismic excitation. Furthermore, two distinct lateral load distribution patterns are adopted in the nonlinear static (pushover) analyses. The first pattern, denoted as PUSH-1, and the second pattern, referred to as PUSH-2, are defined based on different assumptions regarding the distribution of seismic forces along the height of the structure. A detailed description of these loading patterns is provided in Section 4. Also, more details of the framing plan of the studied RC building are presented in the appendix.

Table 1. Identification and naming of load combinations for pushover analysis

Direction	Load Combination	Case	Spectrum X	Spectrum Y	Uniform X/ Y
X	Qu = 0.9QD + QE	0.9-PUSH 1-X	1	0.3	-
		N-0.9-PUSH 1-X	-1	-0.3	-
		0.9-PUSH 2-X	-	-	1/0.3
		N-0.9-PUSH 2-X	-	-	-1/-0.3
	Qu = 1.1(QD + QL) + QE	1.1-PUSH 1-X	1	0.3	-
		N-1.1-PUSH 1-X	-1	-0.3	-
		1.1-PUSH 2-X	-	-	1/0.3
		N-1.1-PUSH 2-X	-	-	-1/-0.3
Y	Qu = 0.9QD + QE	0.9-PUSH 1-Y	1	0.3	-
		N-0.9-PUSH 1-Y	-1	-0.3	-
		0.9-PUSH 2-Y	-	-	1/0.3
		N-0.9-PUSH 2-Y	-	-	-1/-0.3
	Qu = 1.1(QD + QL) + QE	1.1-PUSH 1-Y	1	0.3	-
		N-1.1-PUSH 1-Y	-1	-0.3	-
		1.1-PUSH 2-Y	-	-	1/0.3
		N-1.1-PUSH 2-Y	-	-	-1/-0.3

4. Nonlinear Static Analysis

4.1. General Overview

The investigated structure is a ten-story, three-dimensional reinforced-concrete building with a plan-irregular L-shaped configuration. The building has a uniform story height of 3.2 m and uniform bay lengths of 5 m. The overall plan dimensions are 20 m×20 m, with a 10 m×10 m re-entrant corner opening at the intersection of the two principal plan directions. The reinforced-concrete members are modeled using a concrete compressive strength of F'_c= 25 MPa and reinforcing steel with a yield strength of F_y= 400 MPa. The details of beam and column cross-sections are presented in the appendix. The steel braces are modeled using square hollow structural sections with dimensions of 200×200×10 mm and a nominal yield strength of F_y= 345 MPa. The floor system is assumed to act as a rigid diaphragm, and the beam–column connections are modeled as rigid joints. A damping ratio of 5% of critical damping is adopted for the dynamic analyses. Flexural plastic hinges are assigned at both ends of the beams, while axial–flexural interaction hinges are assigned at the top and bottom ends of the columns. The steel braces are placed in the selected perimeter bays and connected to the surrounding reinforced-concrete frame through concentrically connected brace joints. A three-dimensional numerical model is developed for the nonlinear static (pushover) analysis of the structure. The floor diaphragms, as well as beam-to-column joints, are assumed to be rigid and fully constrained, ensuring full compatibility of deformations across the structural system. The nonlinear response of RC members is simulated through the incorporation of plastic hinge properties [30–32]. Flexural plastic hinges are assigned to beams at two critical locations, namely the start and end regions, in order to capture the potential development of inelastic behavior along the member length. For columns, coupled axial–flexural interaction hinges are defined at both the top and bottom ends to properly represent the combined effects of axial load and bending moments under seismic loading. The modeling parameters, as well as the acceptance criteria for nonlinear analysis of RC beam elements, are summarized in Table 2. Although the default formulation in ETABS [33] is based on average values derived from the first four rows of this table, a more precise calibration of hinge properties is carried out in this study. Specifically, an external Excel-based computational tool is developed to accurately compute hinge parameters in accordance with the tabulated values, ensuring improved numerical reliability.

Table 2. Modeling parameters and acceptance criteria for nonlinear procedures for RC beams [32]

Flexure-Controlled Beams		$3.77\dfrac{V}{b_w d\sqrt{f_c'}}$	a	b	c	IO	LS	CP
$\dfrac{\rho-\rho'}{\rho_{bal}}$	Transverse reinforcement							
≤0.0	NC	≤3	0.02	0.03	0.2	0.005	0.01	0.02
≤0.0	NC	≤6	0.01	0.015	0.2	0.0015	0.005	0.01
≥0.5	NC	≤3	0.01	0.015	0.2	0.005	0.01	0.01
≥0.5	NC	≤6	0.005	0.01	0.2	0.0015	0.005	0.005

Similarly, the plastic hinge properties for column elements are defined based on Table 3, which corresponds to axial, moment interaction behavior in concrete members. The nonlinear moment, rotation relationships are explicitly incorporated into the hinge definitions to capture post-yield behavior and stiffness degradation. Since the structure is designed according to special ductility requirements, all detailing provisions related to transverse reinforcement are satisfied, ensuring adequate confinement in critical regions of the columns. Consequently, the members meet the required ductility and confinement criteria specified in the relevant design provisions. Finally, all frame elements are considered as primary load-resisting members due to their simultaneous participation in both gravity and lateral load-carrying mechanisms, and therefore their nonlinear behavior plays a crucial role in the overall seismic response of the structure.

In the numerical model, the steel braces were connected to the existing reinforced-concrete frame at the beam–column joint regions through idealized steel gusset-plate connections. The brace-to frame connections were modeled as pinned connections, allowing the braces to carry predominantly axial tension and compression forces. The connection behavior was not modeled explicitly in the global analysis; therefore, the reported results represent the response of the braced structural system assuming that the brace connections possess adequate strength and ductility. In practice, the gusset plates, welds, bolts or post-installed anchors, and the surrounding reinforced-concrete members should be designed for the governing brace forces, including the required checks for steel failure, anchor failure, concrete breakout, local crushing, and joint-region damage. The connection design should comply with AISC 360 [34], the seismic provisions of AISC 341[35], the anchorage provisions of ACI 318 [36], and the performance-based rehabilitation principles of ASCE 41 [30].

Table 3. Modeling parameters and acceptance criteria for nonlinear procedures for RC columns [32]

Columns Controlled by Shear								
$\frac{P}{A_g f_c'}$	Transverse Reinforcement	$3.77\frac{V}{b_w d\sqrt{f_c'}}$	a	b	c	IO	LS	CP
≤ 0.1	NC	≤ 3	0.006	0.015	0.2	0.005	0.005	0.006
≤ 0.1	NC	≥ 6	0.005	0.012	0.2	0.005	0.004	0.005
≥ 0.4	NC	≤ 3	0.003	0.01	0.2	0.002	0.002	0.003
≥ 0.4	NC	≥ 6	0.002	0.008	0.2	0.002	0.002	0.002

4.2. Pre-Analysis of Incremental Loading with Gravity Loads

For structures analyzed using nonlinear modeling, each load combination must be evaluated independently from the outset, as the superposition principle is not applicable. Accordingly, gravity loads are initially imposed on the structure, followed by the incremental application of lateral loads. The upper and lower bounds of the gravity loads are defined as follows, where Q_D and Q_L denote the dead and live loads, respectively. The ultimate load combinations considered in the analysis are expressed in equations 1 and 2:

$$Q_U=1.1(Q_D+Q_L)+Q_g \tag{1}$$

$$Q_U=0.9Q_D+Q_g \tag{2}$$

4.3. Lateral Load Distribution

In nonlinear static (pushover) analysis, it is necessary to employ at least two distinct lateral load distributions. In the first approach, given that all structural models investigated in this study exhibit fundamental periods exceeding 1 second, the lateral load pattern is defined in proportion to the lateral forces derived from response spectrum analysis. In the second approach, a uniform lateral load distribution is adopted.

Table 4. Lateral load distribution pattern – Type I

Story	Story Mass (kg)	Lateral Force (N)
roof	5479	2956
10	59981	32362
9	59554	32133
8	59554	32133
7	59876	32305
6	63832	34440
5	64138	34605
4	64554	34830
3	65463	35320
2	66600	35934
1	66884	36087

For the first loading scheme, as reported in Table 4, the lateral force assigned to each story is determined based on the difference between the base shear values of two successive stories. In contrast, in the second scheme referred to as the uniform distribution, the total lateral force, expressed as (V = CW), is allocated to each story in proportion to its weight, as summarized in Table 5.

Table 5. Lateral load distribution pattern – Type II

Story	Story Mass (kg)	Lateral Force (N)
roof	13185	13185
10	80024	66839
9	123040.	43016
8	156894	33853
7	184255	27361
6	209870	25615
5	232564	22693
4	252546	19982
3	270307	17761
2	285220	14912
1	293598	8378

4.4. Target Displacement

A summary of the target displacement calculation is provided in Table 6. First, the target displacement of the structure for Hazard Level 1 is determined for the different pushover load patterns. After defining all elements and components of the nonlinear model, an initial nonlinear analysis is performed to compute the initial displacement, and the base shear, displacement curve of the structure is obtained. Based on this curve, an idealized bilinear representation of the structural behavior is derived. To determine the performance point using the capacity method, both the capacity curve (pushover curve) and the elastic response spectrum with 5% damping are converted, through a set of relationships, into spectral displacement (S_d) and spectral acceleration (S_a) coordinates. The intersection of the elastic response spectrum (in spectral acceleration–period format) and the capacity curve (expressed in base shear–displacement format) identifies the performance point of the structure. After determining the performance point for each pushover pattern, the target displacement of the structure is obtained. PUSH-1 refers to the first lateral load distribution pattern, and PUSH-2 refers to the second pattern. The code-recommended equation for calculating the target displacement is presented in equation 3:

$$\delta_t = C_0 C_1 C_2 C_3 S_a (T_e^2) g/(4\pi^2) \tag{3}$$

Due to the structural asymmetry, lateral loads must be applied separately in the x and y directions. The relationship between base shear and the displacement of the control point must be recorded at every load increment until reaching at least 1.5 times the target displacement. The roof center of mass is selected as the displacement control point.

Table 6. Determination of target displacements for the pushover analysis of the structure

Str.	Dir.	Load Comb.	Case	C_{0_1}	C_{0_2}	C_1	C_2	C_3	T_e (s)	B	S_a (g)	δt (m)
S1-10	X	$Qu = 0.9Q_D + Q_g$	PUSH-1	1.3	---	1	1	1	2.897	0.775	0.128	0.347045
			PUSH-2	---	1.2	1	1	1	2.438	0.869	0.164	0.290688
		$Qu = 1.1(Q_D + Q_L) + Q_g$	PUSH-1	1.3	---	1	1	1	2.931	0.769	0.126	0.349688
			PUSH-2	---	1.2	1	1	1	2.464	0.863	0.162	0.2933
	Y	$Qu = 0.9Q_D + Q_g$	PUSH-1	1.3	---	1	1	1	1.764	1.078	0.154	0.154809
			PUSH-2	---	1.2	1	1	1	1.595	1.153	0.23	0.174488
		$Qu = 1.1(Q_D + Q_L) + Q_g$	PUSH-1	1.3	---	1	1	1	1.633	1.135	0.154	0.13267
			PUSH-2	---	1.2	1	1	1	1.536	1.183	0.226	0.159004

4.5. Retrofit Objective

The retrofit objective defines the desired performance level of the structure during a strong earthquake and is determined by a combination of hazard levels and performance levels. Considering the occupancy category of the building, the retrofit objective is selected as Basic Performance Level, which requires that Life Safety performance be achieved under a Hazard Level 1 earthquake.

4.6. Results of the Initial Model Analysis

In the nonlinear static analysis, after initiating the pushover procedure, the lateral load is applied incrementally until the roof displacement reaches the prescribed target displacement, or the structure collapses before reaching that value. Due to the large number of load combinations, only a sample of the loading cases listed in Table 1 is presented, showing the capacity curves and the pattern of plastic hinge formation in the structure. Figure 2 presents the pushover capacity curve of the original structure under load case 1.1 PUSH 1 X, expressed in terms of base shear versus roof displacement. The curve shows an initial nearly linear branch, indicating that the structure behaves elastically with relatively high initial lateral stiffness under low displacement demands. As the lateral load increases, the slope of the curve gradually decreases, reflecting the onset of nonlinear behavior and the progressive formation of plastic hinges in the structural members. The continuation of the curve beyond the initial linear range indicates that the structure possesses a certain degree of inelastic deformation capacity. However, the reduction in slope suggests stiffness degradation as damage accumulates. Based on the reported pushover results for this load case, the maximum displacement reaches approximately 0.4176 m, while the maximum base shear is approximately 472.669 kN. These values indicate that the unretrofitted L-shaped reinforced-concrete structure can develop a moderate lateral load capacity, but at the cost of a relatively large displacement demand.

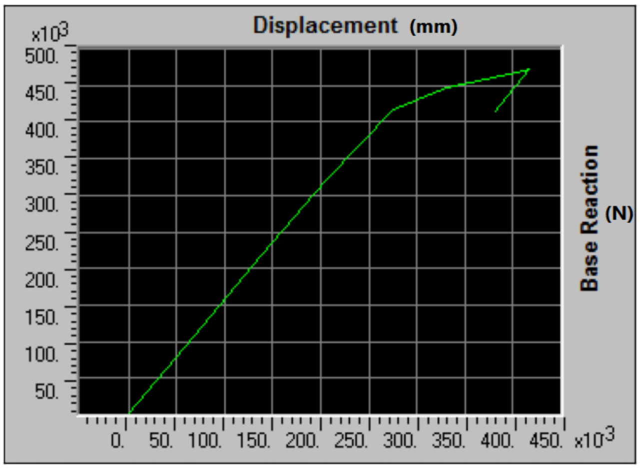

Fig. 2. Capacity curve of the structure under load case 1.1-PUSH-1-X

Figure 3 illustrates the distribution and performance levels of plastic hinges in the original structure under load case 1.1 PUSH 1 X. The hinge pattern indicates that nonlinear deformation is concentrated primarily in the upper stories. At Story 6, several hinges are at performance point B, indicating the initiation of yielding. At Story 7, hinges are mainly within the B–IO range, which reflects limited inelastic action and relatively low damage. However, at Stories 8 to 10, a considerable number of hinges reach the CP (Collapse Prevention) level, demonstrating substantial inelastic demand and severe local damage in these levels. Moreover, a small number of hinges at the roof level reach point D, indicating that the deformation demand in some members exceeds the Collapse Prevention range. No widespread hinges are observed in the E range, suggesting that complete member failure is not dominant under the applied pushover load case. Nevertheless, the concentration of CP- and D-level hinges in the upper stories indicates an unfavorable damage distribution and limited seismic performance of the unretrofitted L-shaped building. This response confirms the need for seismic strengthening to control inelastic deformations and prevent the progression of local damage beyond acceptable performance limits.

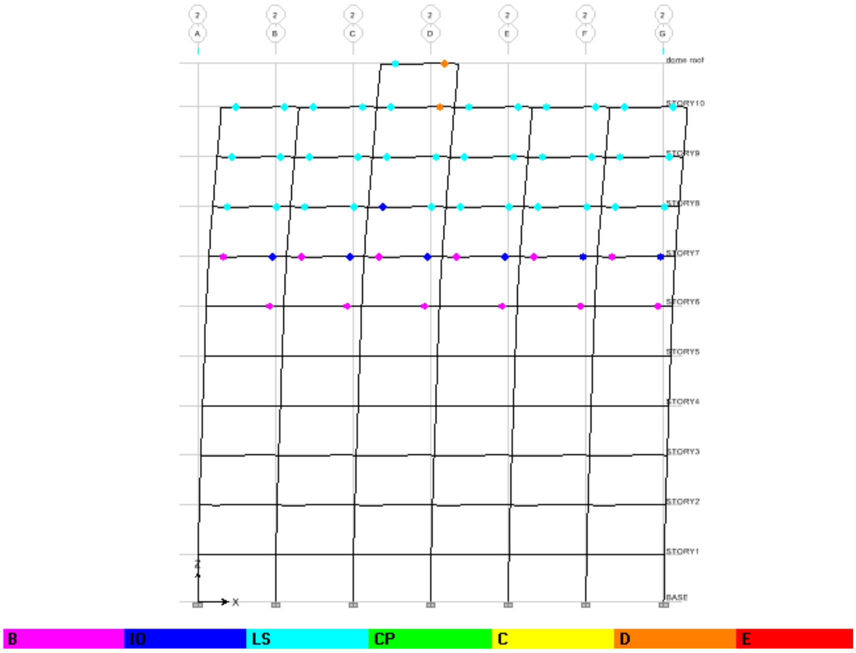

Fig. 3. Pattern of plastic hinge formation in the structure under load case 1.1-PUSH-1-X

The progression of plastic hinge formation under the 1.1 PUSH 1 X load case is summarized in Table 7. The structure maintains elastic behavior until a displacement of approximately 0.139 m (Step 2), where the first two hinges enter the B-IO range. As the lateral displacement increases to 0.275 m (Step 4), a significant transition occurs, with 96 hinges reaching the IO-LS level and 5 hinges reaching the LS-CP performance level. A critical point in the structural response is observed at Step 5 (Displacement = 0.331 m), where the number of hinges at the CP (Collapse Prevention) level jumps to 129. This rapid progression indicates a loss of redundancy and severe localized damage.

Table 7. Plastic hinge formation status of the structure under load case 1.1-PUSH-1-X

Step	Displacement (m)	Base Force (N)	A-B	B-IO	IO-LS	LS-CP	CP-C	C-D	D-E	>E	Total
0	-0.0007893	0.0	1516	0	0	0	0	0	0	0	1516
1	0.0692	108987	1516	0	0	0	0	0	0	0	1516
2	0.1392	217974	1514	2	0	0	0	0	0	0	1516
3	0.2056	321399	1410	106	0	0	0	0	0	0	1516
4	0.275	415999	1345	70	96	5	0	0	0	0	1516
5	0.3318	447906	1307	49	31	129	0	0	0	0	1516
6	0.4107	471047	1304	47	35	128	0	2	0	0	1516
7	0.4176	472669	1304	47	35	126	0	0	4	0	1516
8	0.3797	411808	1516	0	0	0	0	0	0	0	1516

At the ultimate displacement of 0.417 m (Step 7), while the majority of hinges remain in the elastic (A-B) or early yielding stages, 4 hinges reach the D-E range, signifying a total loss of load-carrying capacity in those specific elements. This numerical data corroborates the visual findings in Figure 3, confirming that the unretrofitted L-shaped building undergoes severe inelastic demand, particularly in the upper stories, failing to meet safety requirements before reaching the target displacement. Figure 4 presents the capacity curve of the structure under the 1.1 PUSH 1 Y load case. Both displacement and base reaction are plotted with negative values because the pushover load is applied in the negative Y-direction. The initial portion of the curve is approximately linear, indicating predominantly elastic behavior and an adequate initial lateral stiffness. As the lateral displacement increases, the slope of the curve gradually decreases, reflecting the initiation of yielding, plastic hinge formation, and the development of nonlinear response in the structural members. Overall, the capacity curve demonstrates that the structure develops significant nonlinear behavior under lateral loading in the Y-direction, emphasizing the need to evaluate its deformation capacity and seismic performance at higher displacement demands.

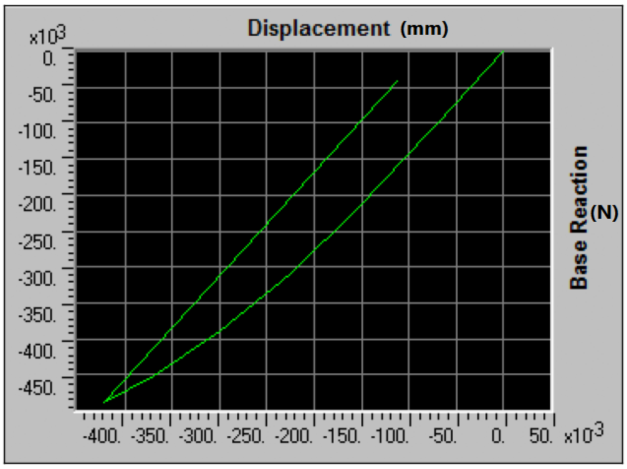

Fig. 4. Capacity curve of the structure under load case N-1.1-PUSH-1-Y

Figure 5 illustrates the distribution of plastic hinges in the structure under the 1.1 PUSH 1 Y load case. The plastic hinges are primarily concentrated in the upper stories, particularly from Stories 6 to 10 and at the roof level. The observed hinges are mainly within the B, IO, and LS performance ranges, indicating the initiation of yielding and the development of moderate inelastic deformation in several structural members. No significant concentration of hinges is observed in the CP, C, D, or E ranges. Therefore, the structure does not exhibit widespread damage associated with the Collapse Prevention or failure states under the considered pushover loading direction. Nevertheless, the absence of plastic hinges in the lower stories and their concentration in the upper part of the building indicate a no uniform distribution of inelastic demand over the height. This response may be related to the plan irregularity of the L-shaped structure and the resulting distribution of lateral stiffness and force demand. Overall, the hinge pattern suggests that the structure experiences localized nonlinear behavior in the upper stories while maintaining a relatively lower damage level in the remaining members under the Y-direction pushover analysis.

Table 8 summarizes the progression of plastic hinge formation in the structure under the 1.1 PUSH 1 Y load case. The total number of monitored hinges remains constant at 1516 throughout the analysis. Initially, all hinges are located within the A–B range, indicating an essentially elastic response. The first inelastic response appears at Step 1, where one hinge enters the B–IO range. With increasing lateral displacement, the number of hinges in the B–IO, IO–LS, and LS–CP ranges gradually increase, indicating the progressive development of nonlinear deformation. At Step 5, corresponding to a displacement of −0.2992 m, 62 hinges are located within the LS–CP range. At the maximum displacement step, Step 7, the structure reaches a base-force magnitude of 487,949 force units at a displacement magnitude of 0.4223 m. At this stage, 1362 hinges, equivalent to approximately 89.84% of the total hinges, remain within the A–B range. Meanwhile, 60, 20, and 71 hinges are located within the B–IO, IO–LS, and LS–CP ranges, respectively. Only two hinges reach the D–E range and one hinge exceed the E limit, while no hinges are observed in the CP–C or C–D ranges. These results indicate that the structure develops a noticeable nonlinear response in the negative Y-direction; however, the critical hinge states are not widespread. The presence of 71 hinges within the LS–CP range reflects a considerable inelastic demand in some structural members, whereas the absence of hinges in the CP–C and C–D ranges suggests that extensive progression beyond the Collapse Prevention level does not occur at the maximum analyzed step. The results are consistent with the hinge distribution shown in Figure 5, where the inelastic demand is mainly concentrated in the upper stories.

In all models, the beams enter the nonlinear range. Most of the plastic hinges formed in the beams fall within the Life Safety (LS) performance level; however, in some cases, these hinges reach the Collapse Prevention (CP) level. Except for the first-story columns—which in some cases enter the Immediate Occupancy (IO) range—the columns in other stories do not enter the nonlinear range. Based on the results of the above tables, and considering that plastic hinges at the Life Safety performance level form before the structure reaches the target displacement—and also given the preservation of column strength, the extensive formation of plastic hinges in beams throughout the structure, and the presence of some residual deformations—it can be concluded that the investigated structures do not satisfy the desired performance objective, which is Life Safety, under the design-level earthquake hazard. Therefore, to achieve a higher performance level, implementing a seismic retrofitting program is justified.

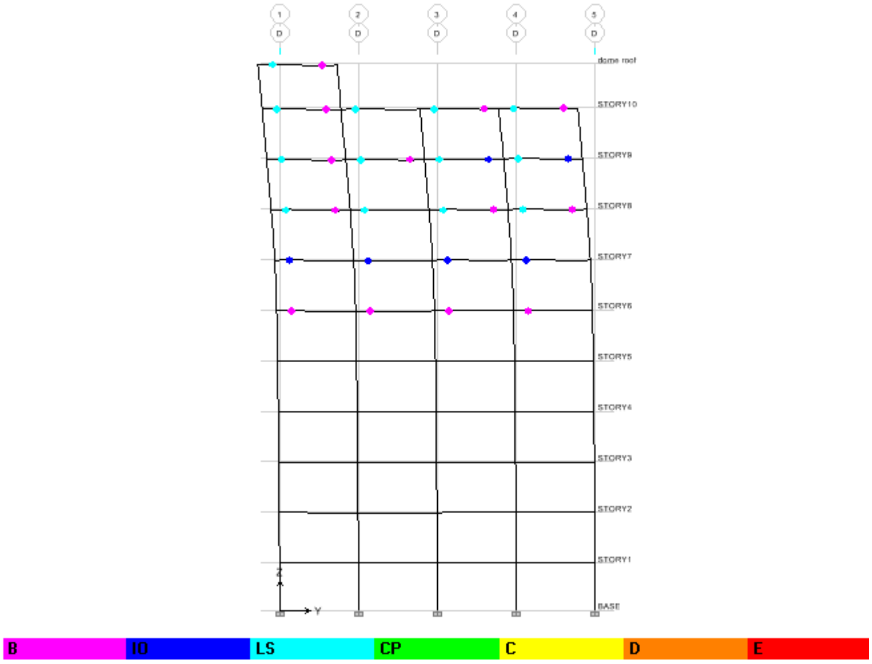

Fig. 5. Pattern of plastic hinge formation in the structure under load case N-1.1-PUSH-1-Y

Table 8. Plastic hinge formation status of the structure under load case N-1.1-PUSH-1-Y

Step	Displacement (m)	Base Force (N)	A-B	B-IO	IO-LS	LS-CP	CP-C	C-D	D-E	>E	TOTAL
0	-6.901E-04	0.0000	1516	0	0	0	0	0	0	0	1516
1	-0.0707	-100269	1515	1	0	0	0	0	0	0	1516
2	-0.0799	-113471	1500	16	0	0	0	0	0	0	1516
3	-0.1528	-216583	1461	41	14	0	0	0	0	0	1516
4	-0.2247	-309884	1431	26	46	13	0	0	0	0	1516
5	-0.2992	-388810	1404	33	17	62	0	0	0	0	1516
6	-0.3694	-451287	1362	60	20	73	0	1	0	0	1516
7	-0.4223	-487949	1362	60	20	71	0	0	2	1	1516
8	-0.1110	-39964	1516	0	0	0	0	0	0	0	1516

5. Nonlinear Dynamic Analysis

5.1. Introduction and Analysis

In this method, the structure is analyzed under a set of recorded or simulated acceleration time histories. The ground motions must be consistent with the rupture mechanism of the seismic source, the corresponding earthquake magnitude, the source-to-site distance, the geological and tectonic characteristics, and the soil layers. Depending on the requirements, the selected records must also be compatible with the design spectrum, or the maximum considered earthquake (MCE) spectrum. Since the structure examined in this study is irregular, the analysis must be performed as a fully three-dimensional inelastic analysis. In this research, three selected ground motions correspond to the Tabas, Northridge, and Landers earthquakes. Their acceleration time histories in the X direction are shown respectively in Figures 6 to 8. The magnitudes of these earthquakes are 7.4, 6.7, and 7.3 (Mw), respectively.

The acceleration records are processed in SeismoSignal and prepared for import into ETABS. Each pair of acceleration time histories must be applied to the structure simultaneously in two orthogonal directions. In the next step, the application direction of each ground motion must be switched, and the critical case should be selected from these two analyses. For example, for the Tabas earthquake, two analysis cases are considered and introduced into the software as TABAS1 and TABAS2. Given the irregularity of the structure, the direction of the applied earthquake loading must be selected so as to produce the maximum possible effect. To account for the maximum seismic impact, 100% of the earthquake force in one direction may be combined with 30% of the earthquake force in the perpendicular direction. For instance, for the Tabas earthquake, the following two load combinations are defined as equations 4 and 5 in the ETABS software:

$$THTABAS1=TABAS1+0.3TABAS2 \tag{4}$$

$$THTABAS2=TABAS2+0.3TABAS1 \tag{5}$$

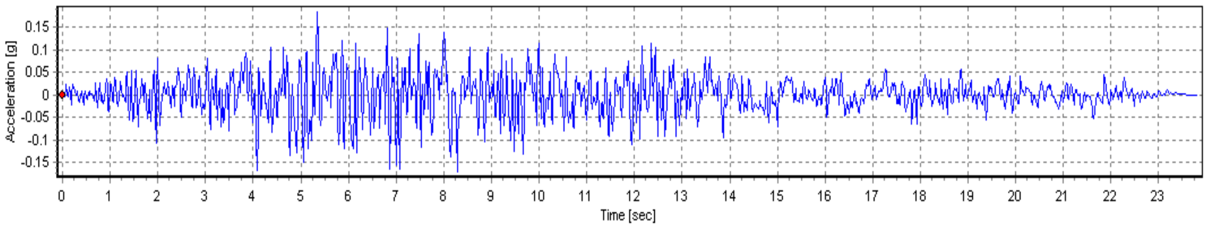

Fig. 6. Acceleration time history of the Tabas earthquake

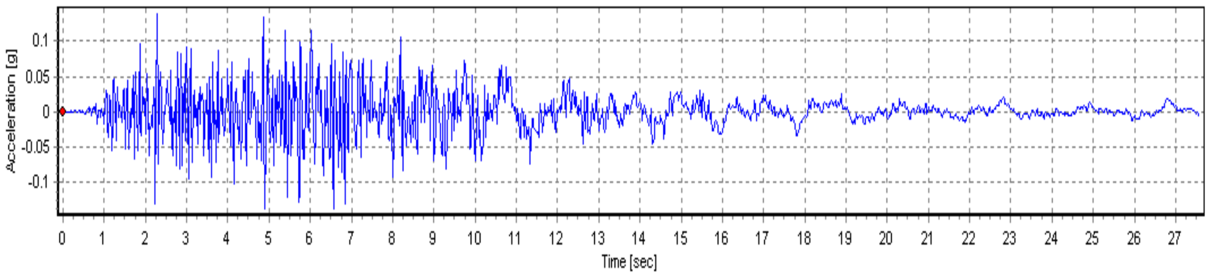

Fig. 7. Acceleration time history of the Northridge earthquake

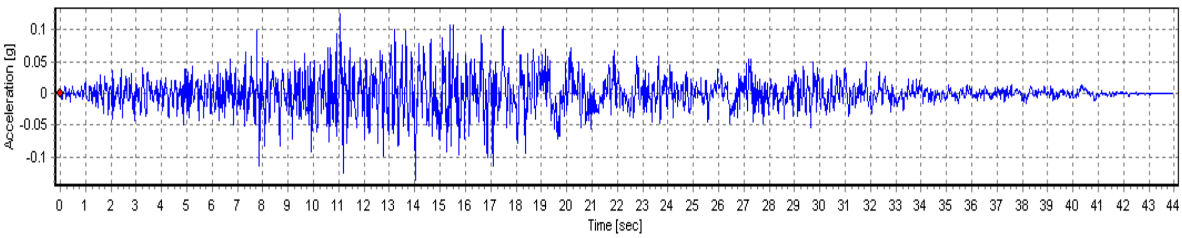

Fig. 8. Acceleration time history of the Landers earthquake

5.2 Evaluation of the Structure in Nonlinear Dynamic Analysis

In a nonlinear analysis of the three-dimensional structural model, a large volume of results is generated at each time step. Given the abundance and complexity of these data, the precise setting of acceptance criteria within the analysis software is of particular importance to ensure accuracy and reliability of the results. Figures 9 to 12 illustrate the deformation response of the structure under the previously mentioned earthquake records.

The results indicate that the original structure experiences significant displacement demands under the selected earthquake records, particularly Landers and Tabas, while Northridge generally induces lower response levels. In the X direction, Type II analysis produces the most severe deformation demand, with peak roof displacement approaching approximately 90 cm, indicating the limited lateral stiffness and deformation control capacity of the as-built configuration.

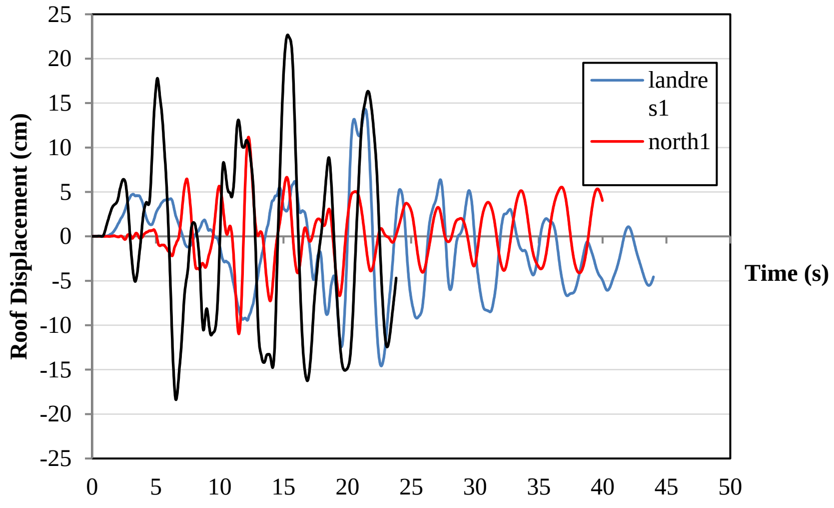

Fig.9. Structural deformation response in the X direction under Type I analysis

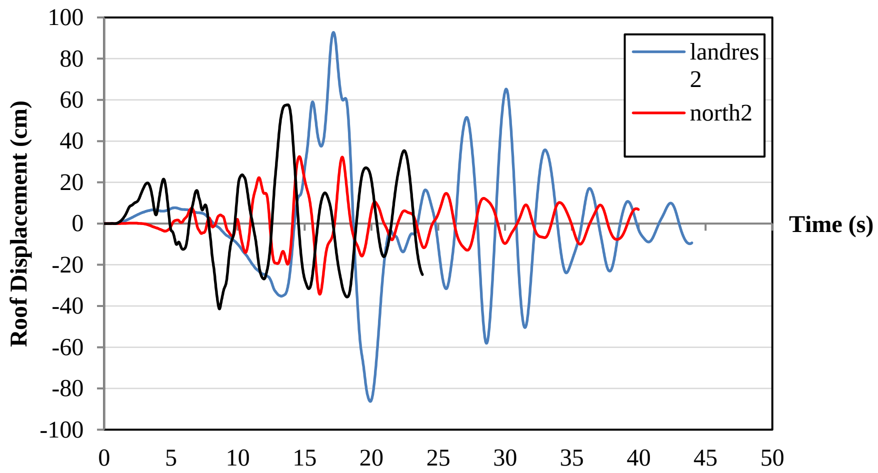

Fig. 10. Structural deformation response in the X direction under Type II analysis

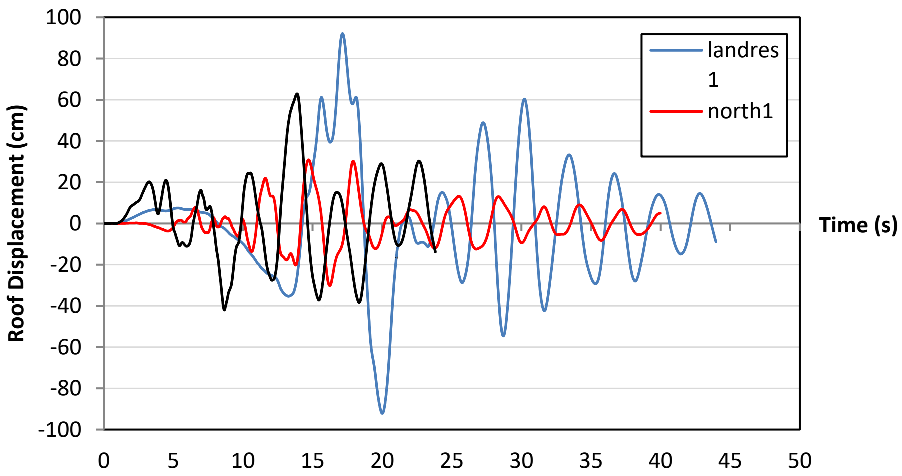

Fig. 11. Structural deformation response in the Y direction under Type I analysis

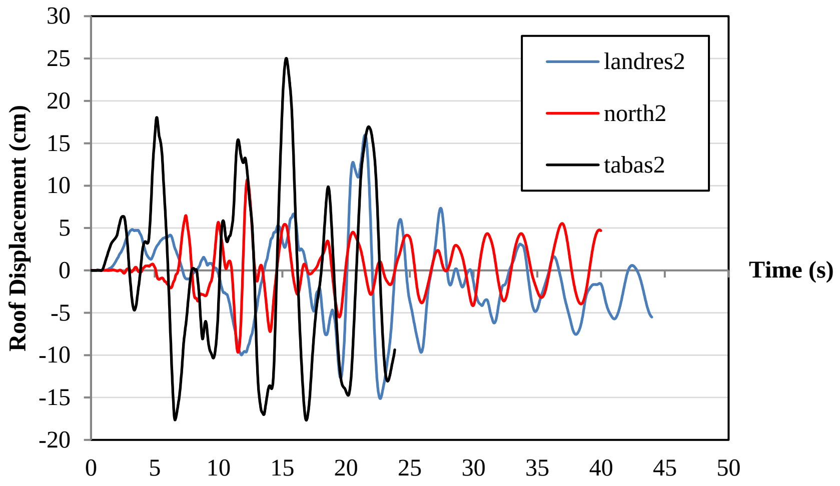

Fig.12. Structural deformation response in the Y direction under Type II analysis

A similar trend is observed in the Y direction, where large displacement amplitudes are also developed under the stronger ground motions. Overall, the response histories confirm that the original building is vulnerable to seismic excitation and exhibits insufficient capacity to control lateral drift, thereby justifying the need for seismic retrofitting using steel bracing systems.

5.3 Determination of the Overall Structural Performance Level Using Nonlinear Dynamic Analysis

Despite the relative agreement between the results of nonlinear dynamic and nonlinear static analyses, because the maximum response values govern in nonlinear dynamic analysis, the results obtained from this method—such as displacements and rotations—are generally larger than those from nonlinear static analysis. Comparing the selected ground motion records indicates that, in most cases, the Northridge earthquake produces smaller responses and less nonlinear behavior in the structure. However, during the Tabas and Landers earthquakes, due to their stronger frequency content and higher energy, the nonlinear behavior of the structure increases and plastic hinges are extensively formed in the beams. In the analyzed structures, no cases of brittle failure or section inadequacy in force-controlled actions were observed. The models show that plastic hinges form in beams prior to columns, confirming the development of the weak-beam–strong-column mechanism, which is the desirable mechanism for preventing structural collapse. Therefore, considering that the beams enter the collapse stage, selecting a performance range below that level for the overall structure appears appropriate. According to the definition, within the Collapse Prevention (CP) performance level, the key structural components are still capable of carrying the required gravity loads; however, the structure is at the threshold of overall collapse. Additionally, large and permanent displacements are expected within this range, which were also observed in the various models investigated in this study. Therefore, similar to the nonlinear static analysis method, the selected performance level is Collapse Prevention (CP).

6. Results of Nonlinear Static Analysis for the Retrofitted Model

The retrofit objective in this study was to improve the seismic performance of the existing plan-irregular L-shaped reinforced-concrete building through enhancement of lateral strength, stiffness, ductility, and overall structural stability. Due to the geometric irregularity of the building plan, the structure is more susceptible to torsional effects, uneven demand distribution, and localized nonlinear damage under seismic excitation. Therefore, a steel bracing system was selected as the retrofit strategy to provide an efficient additional lateral load-resisting mechanism, reduce structural vulnerability, and improve the global response of the building under pushover and nonlinear dynamic analyses. This retrofit objective was defined in accordance with the performance-based rehabilitation philosophy of ASCE 41 [29] and FEMA 356 [30], which are widely used guidelines for seismic evaluation and retrofit of existing buildings. For the retrofitted structure (Figure 13), the initial analysis procedures are carried out in the same manner as for the unretrofitted structure. For example, in the retrofitted structure, the distribution of lateral loads is presented in Tables 9 and 10.

The lateral load distribution results, as detailed in Tables 9 and 10, indicate that the story shear increases progressively from the roof toward the base, reaching its maximum value of 295.653 kN at the first story. This trend is consistent with the expected accumulation of seismic shear forces along the height of the building. The distributed forces are smaller at the roof level and gradually increase in the lower stories, reflecting the vertical transfer of inertial loads. Furthermore, in the uniform distribution pattern (Type II), the applied lateral forces are approximately proportional to the story masses; these masses remain relatively consistent over most floors, showing only minor variations. This confirms that the adopted load pattern provides a rational representation of the seismic demand along the building's height. Table 11 presents the calculated target displacement parameters for the retrofitted structure under different loading combinations in both the X and Y directions.

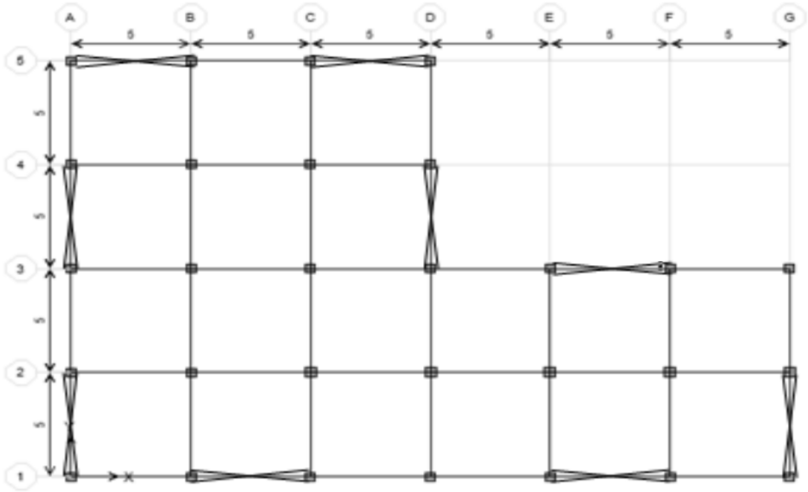

Fig. 13. Plan view of bracing layout for the retrofitted structure

Table 9. Lateral load distribution pattern based on the linear dynamic method (Type I distribution)

Story	Story Shear (N)	Distributed Force (N)
roof	13387	13387
10	77328	63940
9	124327	46999
8	156403	32075
7	180202	23799
6	202623	22421
5	225327	22703
4	248107	22780
3	269387	21279
2	286690	17302
1	295653	8963

The results demonstrate that the target displacement in the Y-direction is consistently larger than in the X-direction, with a maximum value of 0.235 m compared to 0.166 m in the X-direction. This suggests that the structure possesses greater flexibility and undergoes larger lateral deformations in the Y-direction. The effective period (T_e) is also higher in the Y-direction, reaching 1.818 s, whereas it is approximately 1.40 s in the X-direction, which further supports this interpretation. In addition, the damping-related modification factor (B) varies between approximately 1.057 and 1.408, indicating the influence of effective damping on the target displacement evaluation. Overall, these results demonstrate that inherent directional stiffness differences significantly affect the seismic displacement demand of the retrofitted L-shaped building.

Table 10. Lateral load distribution pattern based on uniform distribution (Type II distribution)

Story	Story Mass (kg)	Distributed Force (N)
roof	5478	2955
10	60185	32473
9	59963	32353
8	59963	32353
7	60285	32526
6	64275	34680
5	64615	34863
4	65032	35088
3	65941	35578
2	67078	36191
1	67357	36342

Table 11. Determination of target displacements for pushover analysis

Str.	Dir.	Load Comb.	Case	C_{0_1}	C_{0_2}	C_1	C_2	C_3	T_e (s)	B	S_a (g)	δt (m)
S1-10/ Retrofitted	X	$Qu = 0.9Q_D + Q_g$	PUSH-1	1.3	---	1	1	1	1.407	1.254	0.258	0.165
			PUSH-2	---	1.2	1	1	1	1.182	1.408	0.313	0.130
		$Qu = 1.1(Q_D + Q_L) + Q_g$	PUSH-1	1.3	---	1	1	1	1.41	1.252	0.259	0.166
			PUSH-2	---	1.2	1	1	1	1.185	1.406	0.314	0.131
	Y	$Qu = 0.9Q_D + Q_g$	PUSH-1	1.3	---	1	1	1	1.818	1.057	0.22	0.235
			PUSH-2	---	1.2	1	1	1	1.516	1.193	0.259	0.178
		$Qu = 1.1(Q_D + Q_L) + Q_g$	PUSH-1	1.3	---	1	1	1	1.792	1.067	0.223	0.231
			PUSH-2	---	1.2	1	1	1	1.526	1.188	0.26	0.181

As observed, due to the reduction in the fundamental period and the increase in structural stiffness, a significant decrease in the target displacement values has occurred. Although the reduction in target displacements is an important step toward improving the structural performance level, it cannot, by itself, be considered an indicator of better overall performance. Instead, the acceptance criteria and the story displacement values obtained after the analysis are the primary measures for determining the updated performance level of the structures. The analysis of the retrofitted structures shows that, as expected, displacements have decreased and force demand has increased, with the additional forces being absorbed by the bracing members. In this section, due to the large number of load combinations, only a few selected cases from Table 1 are presented as examples, including the capacity curve and the pattern of plastic hinge formation in the structure. Figures 14 and 15 show the capacity curves of the retrofitted structure under the 1.1(QD+QL) +Qg load combination and the PUSH-2 load pattern in the X- and Y-directions, respectively. The structure develops an approximate base reaction of 580 kN at a displacement of nearly 60 mm in the X-direction, whereas the corresponding response in the Y-direction reaches approximately 560 kN at a displacement of about 75–78 mm. The greater displacement demand in the Y-direction reflects the lower effective stiffness associated with the plan-irregular configuration. In both directions, the capacity curves exhibit a stable response without a pronounced sudden strength loss. As shown in Figure 16, plastic hinges are predominantly within the B–IO performance range, while only a limited number of hinges in the lower and intermediate stories approach the LS or CP ranges. The absence of a widespread column hinge mechanism and the concentration of inelastic response mainly in beams indicate a favorable and controlled damage distribution. These results confirm the effectiveness of the steel bracing system in improving the lateral resistance, deformation control, and overall seismic performance of the L-shaped RC building. Tables 12 and 13 indicate that the retrofitted structure exhibits a stable and ductile hinge formation pattern under both pushover load cases. In the X-direction, the structure attains a peak base force of 593.901 kN at a displacement of 0.0656 m, while the number of hinges in the B–IO and D–E ranges remain limited, with no progression to severe collapse states. In the Y-direction, the maximum base force is 554.630 kN at a displacement of 0.0747 m, and hinge accumulation is similarly controlled, although the Y-direction shows slightly larger deformation demand. In both cases, the dominance of hinges in the A–B state and the absence of widespread severe damage confirm the effectiveness of the steel bracing system in reducing damage concentration and improving overall seismic performance.

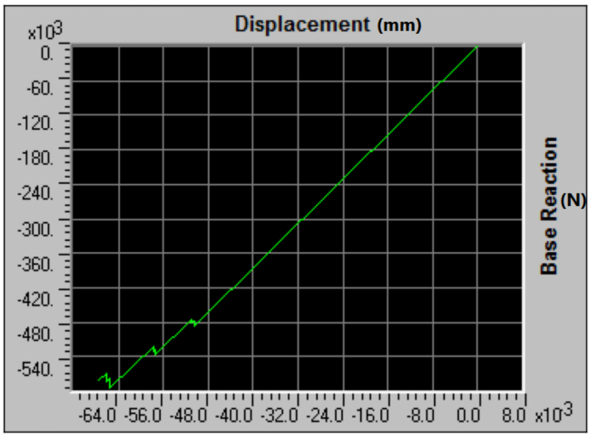

Fig. 14. Capacity curve of the retrofitted structure under load case N-1.1-PUSH 2-X

Table 12. Plastic hinge formation status of the retrofitted structure under load case N-1.1-PUSH 2-X

Step	Displacement (m)	Base Force (N)	A-B	B-IO	IO-LS	LS-CP	CP-C	C-D	D-E	>E	TOTAL
0	0.0	0.0	1694	2	0	0	0	0	0	0	1696
1	-0.0501	-483475	1694	2	0	0	0	0	0	0	1696
2	-0.0505	-487301	1691	2	0	0	0	0	3	0	1696
3	-0.0505	-478870	1691	0	1	0	0	1	3	0	1696
4	-0.0509	-482453	1691	0	0	0	0	2	5	0	1696
5	-0.0509	-475992	1689	0	2	0	0	2	5	0	1696
6	-0.0574	-536128	1686	0	2	0	0	0	8	0	1696
7	-0.0574	-527664	1686	0	1	0	0	1	8	0	1696
8	-0.0576	-529514	1686	0	0	0	0	0	10	0	1696
9	-0.0576	-522872	1679	3	0	0	0	4	10	0	1696
10	-0.0656	-593901	1669	11	0	0	0	0	16	0	1696
11	-0.0656	-577929	1668	10	1	0	0	1	16	0	1696
12	-0.0661	-582373	1665	11	0	0	0	0	20	0	1696
13	-0.0661	-569907	1664	12	0	0	0	0	20	0	1696
14	-0.0677	-584761	1696	0	0	0	0	0	0	0	1696

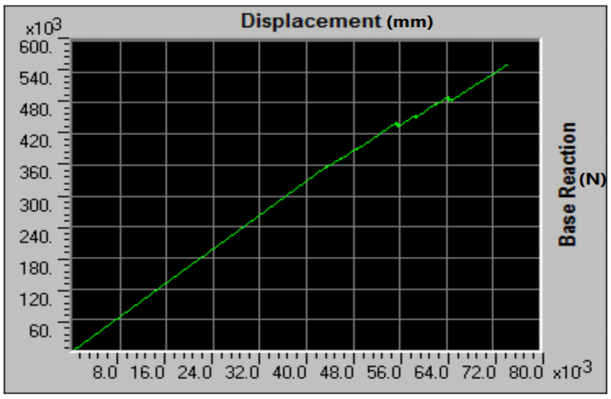

Fig. 15. Capacity curve of the retrofitted structure under load case 1.1-PUSH 2-Y

Table 13. Plastic hinge formation status of the retrofitted structure under load case 1.1-PUSH 2-Y

Step	Displacement (m)	Base Force (N)	A-B	B-IO	IO-LS	LS-CP	CP-C	C-D	D-E	>E	TOTAL
0	0.0000	0.0000	1695	1	0	0	0	0	0	0	1696
1	0.0431	353959	1695	0	0	0	0	1	0	0	1696
2	0.0435	356761	1695	0	0	0	0	0	1	0	1696
3	0.0435	354352	1694	0	0	0	0	1	1	0	1696
4	0.0458	373243	1694	0	0	0	0	0	2	0	1696
5	0.0458	370527	1693	0	0	0	0	1	2	0	1696
6	0.0486	393061	1693	0	0	0	0	0	3	0	1696
7	0.0486	390532	1692	0	0	0	0	1	3	0	1696
8	0.0511	410597	1692	0	0	0	0	0	4	0	1696
9	0.0511	407949	1689	0	1	0	0	2	4	0	1696
10	0.0554	441589	1687	0	3	0	0	0	6	0	1696
11	0.0554	437032	1687	0	2	0	0	1	6	0	1696
12	0.0557	439201	1687	0	1	0	0	0	8	0	1696
13	0.0557	434002	1686	0	1	0	0	1	8	0	1696
14	0.0587	457589	1686	0	0	0	0	0	10	0	1696
15	0.0587	450713	1683	2	0	0	0	1	10	0	1696
16	0.0622	477089	1683	2	0	0	0	0	11	0	1696
17	0.0622	475317	1681	2	1	0	0	1	11	0	1696
18	0.0643	491190	1680	1	1	0	0	0	14	0	1696
19	0.0643	482861	1680	1	0	0	0	1	14	0	1696
20	0.0648	486753	1680	1	0	0	0	0	15	0	1696
21	0.0648	484548	1679	1	0	0	0	1	15	0	1696
22	0.0667	498405	1679	1	0	0	0	0	16	0	1696
23	0.0667	496562	1675	3	0	0	0	2	16	0	1696
24	0.0747	554630	1696	0	0	0	0	0	0	0	1696

Based on the general acceptance criteria in the nonlinear static (pushover) method, an improvement in the overall structural weakness is observed, and in most cases, the performance level of the structure improves from instability and collapse prevention to the Life Safety (LS) performance level. After retrofitting the structure using steel bracing, plastic hinges form in the beams of most stories at the target displacement. In the first loading type, and after retrofitting, the majority of damage is concentrated in the beams, while the columns generally remain undamaged under this loading. In most cases, the members are able to satisfy the Life Safety performance level. The maximum damage is observed in the beams of the braced bays, which represent the minimum performance level.

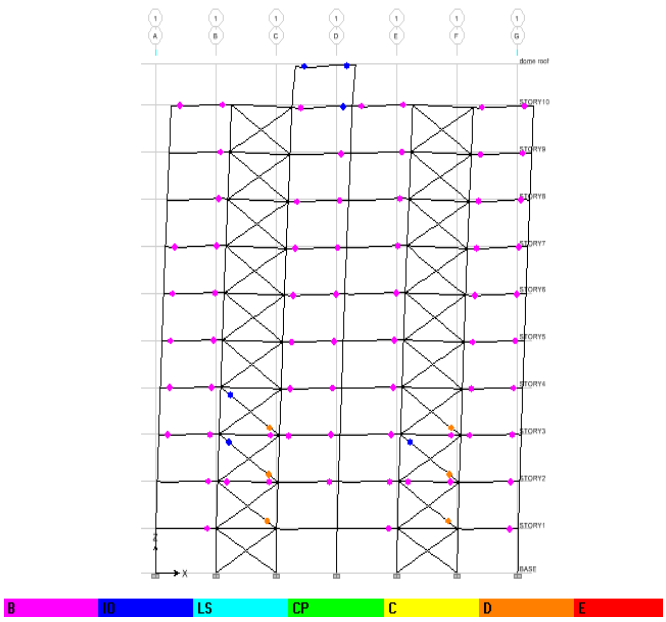

Fig. 16. Plastic hinge formation pattern of the retrofitted structure

The compression braces in most stories experience buckling. Step-by-step loading shows that after brace buckling, plastic hinges form in the beams of the braced bays, and with progressive loading, the plastic rotations of the beams in the middle bays increase, eventually extending plastic hinges into adjacent beams as the lateral load continues. The tension braces yielded only in a few cases and only under the first loading pattern at the target displacement. Under the second loading type, the performance level inferred from the hinge formation pattern indicates that the columns of the lower stories experience greater damage. The results also show that the highest damage still occurs in the beams of the braced bays. However, the distribution and performance level of the plastic hinges indicate that the damage remains at an acceptable and controlled level. The minimum performance level achieved by the members corresponds to Life Safety (LS). The braces in the top story do not buckle, indicating the overstrength of the upper story in these frames. Additionally, removal of these braces would lead to the formation of plastic hinges at the Immediate Occupancy (IO) performance level in the beams of the upper stories. Brace buckling in most stories occurs before reaching the target displacement, but tension braces rarely yield. Reviewing the results shows that adding steel bracing to RC frames axializes the bending demands transferred to the columns, thereby reducing their stress ratios to values below one. Furthermore, the axialization of seismic loads not only decreases column stress ratios to allowable limits but also shifts plastic hinge formation from columns to beams, protecting the columns from significant damage. Overall, based on the conducted evaluations, the structure—after retrofitting with steel bracing—experiences an improved performance level and satisfies the Life Safety performance objective. Table 9 also confirms that within the Life Safety range, no plastic hinges have formed.

7. Results of Nonlinear Dynamic Analysis for the Retrofitted Model

Using the accelerograms of the mentioned earthquakes, the retrofitted structure is subjected to nonlinear dynamic analysis. The maximum response values obtained in this stage show a significant reduction compared to those of the original (unretrofitted) structure. Figures 17 to 20 illustrate the nonlinear time history response of the retrofitted L-shaped RC building under three selected ground motion records: Landers, Northridge, and Tabas. The results are categorized under two analysis types (Type I and Type II) for both X and Y directions. As shown in Figures 17 and 20, the steel bracing system effectively limits the roof displacement to a range of 10-17 cm for most cases, demonstrating a significant increase in lateral stiffness and energy dissipation capacity. The oscillations are characterized by a rapid decay after the peak acceleration, highlighting the efficiency of the added braces in providing supplemental damping. However, in Figures 18 and 19, the structure exhibits a higher displacement demand under the Landers record, reaching a peak of approximately 70 cm. This response can be attributed to the long-period characteristics of the Landers earthquake which may align with the fundamental period of the irregular structure. Despite these peak values, the retrofitted system maintains its global stability, and no permanent offset (residual displacement) is critically observed, confirming that the bracing system prevents the RC frame from entering a collapsed state under extreme seismic pulses.

Overall, the retrofitted building exhibits larger story displacements than the original one, which indicates an improved deformation capacity and greater ductility rather than a loss of performance. The steel bracing system enables the structure to sustain higher lateral deformation demands while maintaining stable response distribution along the height. In contrast, the original structure reaches its capacity limit earlier and shows a less favorable lateral behavior. In Figures 29 and 30, the capacity curves of the structure before and after retrofitting are presented for two sample load combinations. As seen in these figures, adding the bracing members increases the base shear while the corresponding displacement decreases, and the area under the curve—representing the amount of energy absorbed and dissipated by the structure—also increases. In this method, similar to the nonlinear static procedure, retrofitting the structures results in reduced displacements and an improvement in overall structural performance. In this section, the story displacements are compared under dynamic load distribution and uniform load distribution. Figures 21 to 28 show the story displacement profiles of the original and retrofitted structures under different pushover load cases.

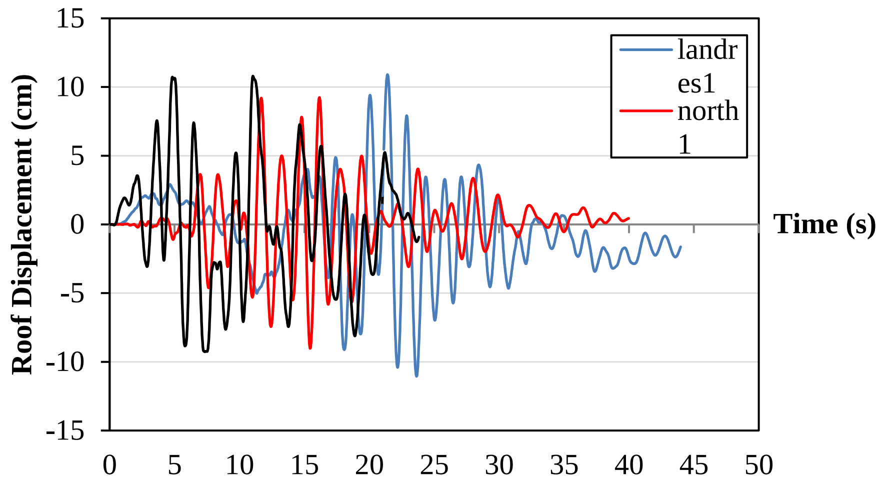

Fig. 17. Structural deformation response in the X direction under Analysis Type I

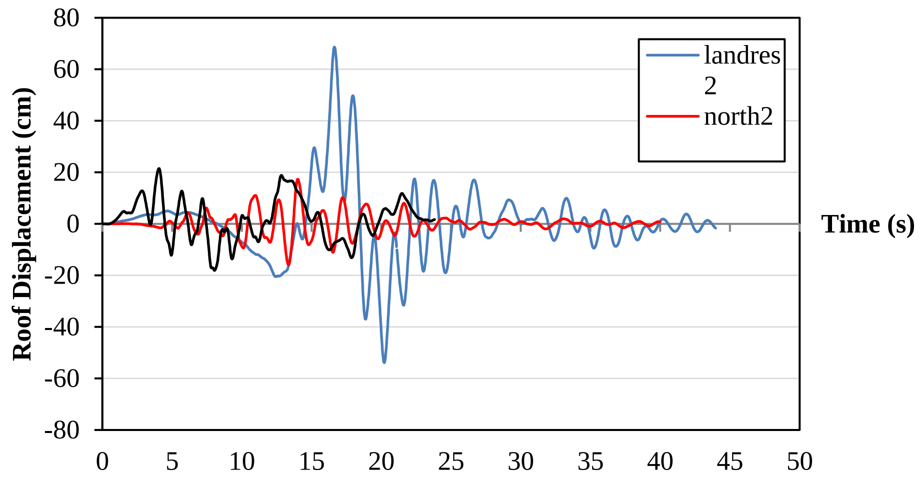

Fig. 18. Structural deformation response in the X direction under Analysis Type II

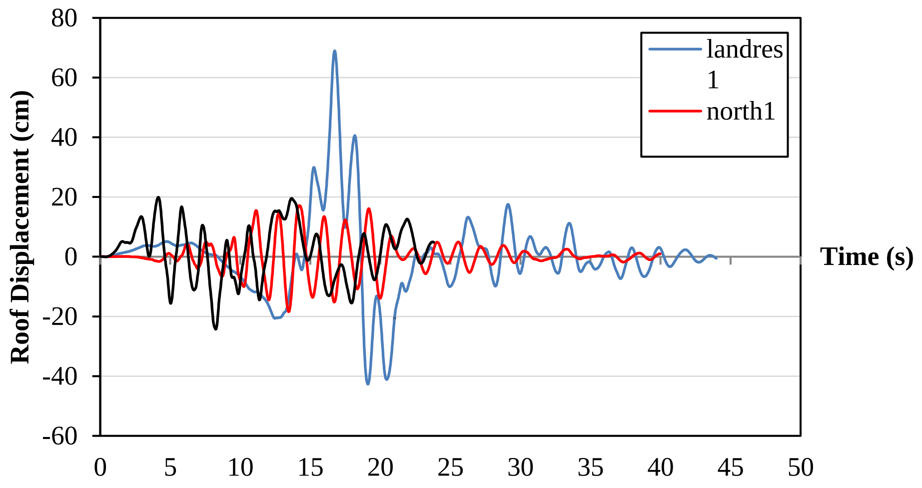

Fig. 19. Structural deformation response in the Y direction under Analysis Type I

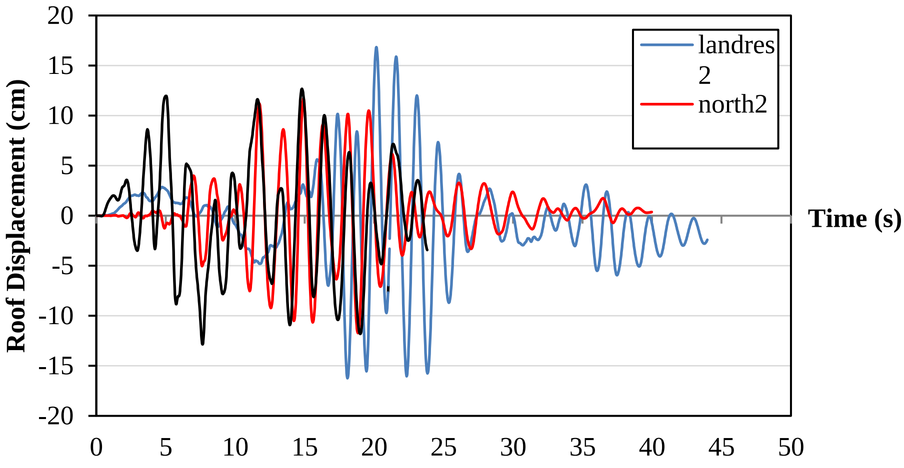

Fig. 20. Structural deformation response in the Y direction under Analysis Type II

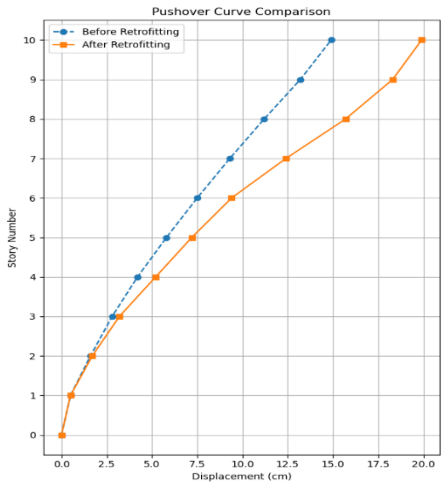

Fig. 21. Story displacements under load case 1.1-PUSH 1-X

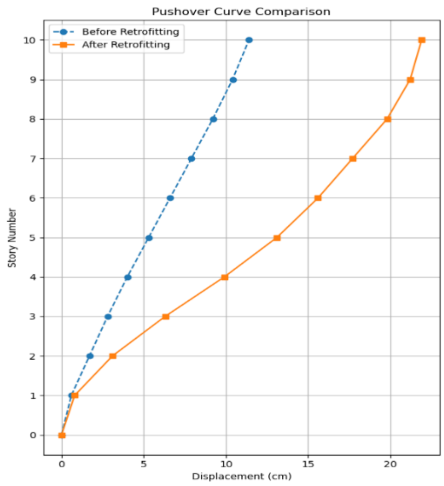

Fig. 22. Story displacements under load case 1.1-PUSH 2-X

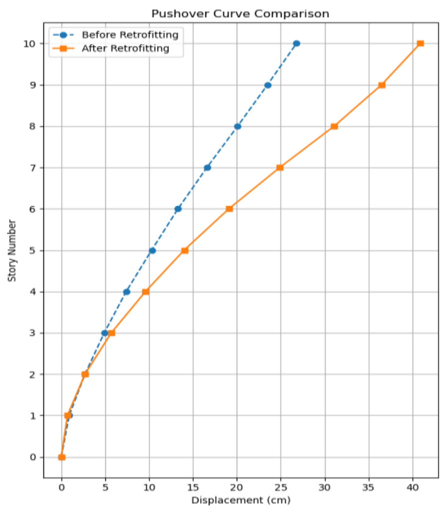

Fig. 23. Story displacements under load case 1.1-PUSH 1-Y

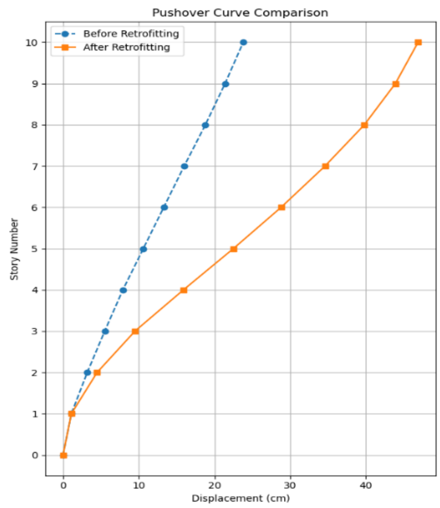

Fig. 24. Story displacements under load case 1.1-PUSH 2-Y

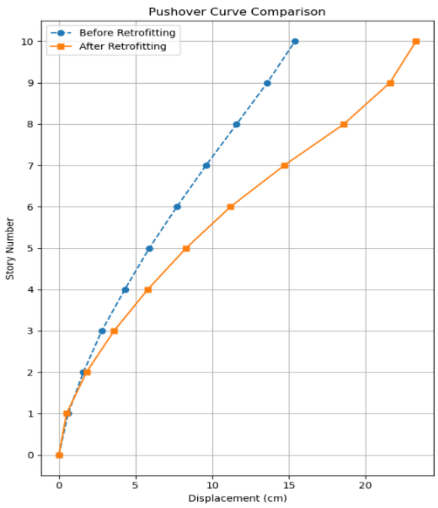

Fig. 25. Story displacements under load case 0.9-PUSH 1-X

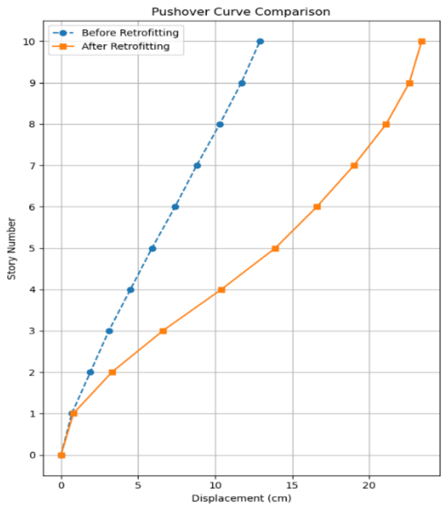

Fig. 26. Story displacements under load case 0.9-PUSH 2-X

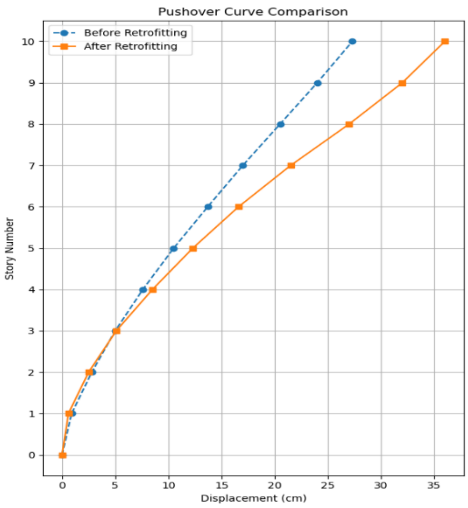

Fig. 27. Story displacements under load case 0.9-PUSH 1-Y

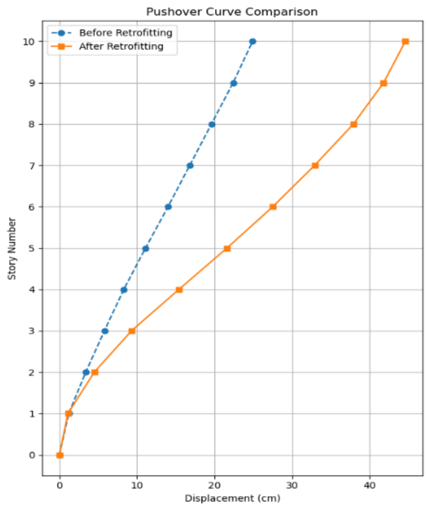

Fig. 28. Story displacements under load case 0.9-PUSH 2-Y

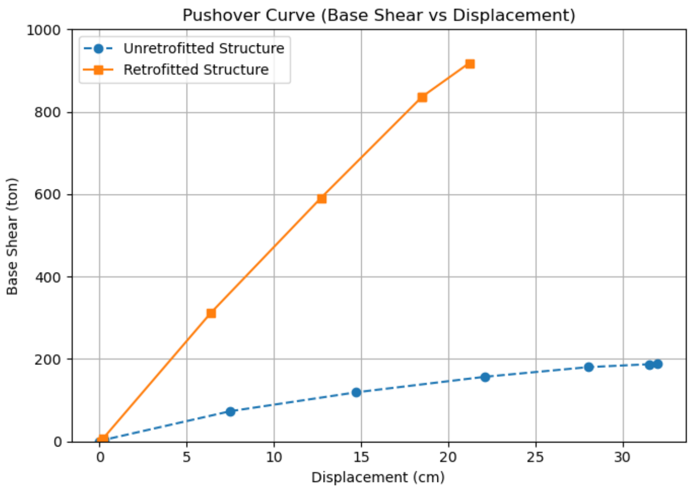

Fig. 29. Comparison of structural capacity curves under load case 0.9-PUSH 1-Y

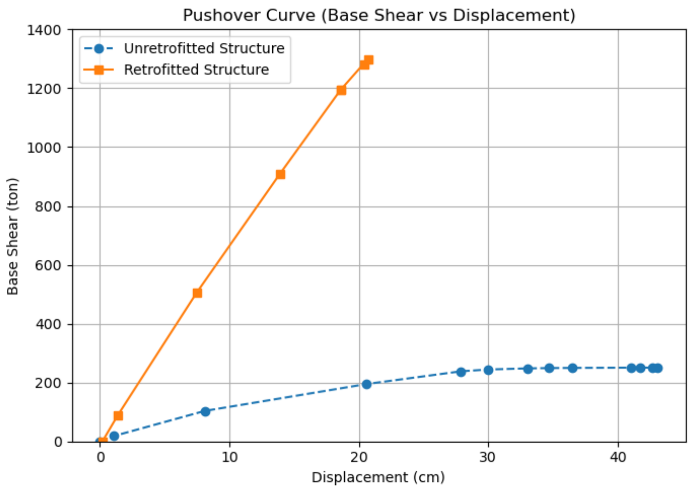

Fig. 30. Comparison of structural capacity curves under load case 1.1-PUSH 2-Y

Furthermore, the increase in the initial slope of the curve indicates an increase in structural stiffness, which in turn causes the seismic forces applied to the structure to increase. However, since the load-carrying capacity of the structure also increases after retrofitting, the retrofitted structures are capable of resisting these higher forces. These figures clearly demonstrate that the retrofitted structure achieves a much higher lateral strength than the unretrofitted one. The results indicate that the retrofitted structure achieves approximately 4.8 and 5.2 times the base-shear capacity of the unretrofitted structure in the respective loading cases, corresponding to increases of approximately 384% and 420%, respectively. These findings demonstrate the substantial contribution of the steel bracing system to the lateral strength and deformation capacity of the L-shaped reinforced-concrete building.

8. Conclusion

This study presented a comprehensive investigation into the seismic performance enhancement of a plan-irregular L-shaped RC building retrofitted with steel bracing systems. Utilizing nonlinear static pushover analysis in accordance with FEMA guidelines, the structural response was meticulously evaluated before and after retrofitting. The methodology employed two distinct lateral load distribution patterns—proportional to the fundamental mode shape and proportional to the story mass—to verify the structural stability and deformation capacity. Based on the comparative numerical and qualitative assessment of the structural behavior, the following conclusions are drawn:

- Installing bracing in the structure increases stiffness and reduces the fundamental period of the structure. This increase in stiffness and reduction in the period lead to an increase in the base shear. However, due to the favorable structural behavior provided by the dual system, the performance level of the model improves.
- Adding steel bracing to RC frames transforms the bending loads applied to the columns into axial forces; therefore, the stress ratios in the columns are reduced to values less than one. The axialization of seismic loads not only reduces the column stress ratios relative to the allowable stresses but also transfers plastic hinge formation from columns to beams. As a result, more than 80% of the columns remain undamaged under this retrofitting method.
- The comparative analysis of the force–displacement (pushover) curves indicate a substantial improvement in structural capacity. The retrofitted model exhibited a base shear capacity increase of approximately 25.6% (from 472.669 kN to 593.901 kN), demonstrating the system's increased resistance to lateral seismic loads.
- The effectiveness of the retrofitting strategy is most evident in the reduction of seismic deformation demand. The target displacement was reduced by approximately 83.8% (from 0.4176 m to 0.0677 m) in the braced model compared to the bare RC frame. This outcome

underscores the efficiency of the dual system in controlling lateral drift and suppressing excessive sway.

- By comparing the performance of beams and columns, it is observed that in the structure retrofitted with steel bracing, fewer plastic hinges form in both beams and columns, leading to improved structural performance.
- Comparison of the force–displacement curves shows that RC structures with bracing provide higher shear capacity than similar structures without bracing, thereby increasing the overall structural capacity.
- In the braced structure, the target displacement is reduced compared with the RC structure without bracing, clearly demonstrating the advantage of the dual system and the interaction between the moment-resisting frame and the bracing system.
- Comparison of the force–displacement curves indicates that, in all cases, the second type of lateral load distribution (proportional to the weight of each story) produces higher base shear values than the first type of lateral load distribution (proportional to the lateral forces obtained from response spectrum analysis).
- The pattern of hinge formation in the retrofitted structure indicates that the use of steel bracing introduces additional forces to the frame at upper stories, leading to the formation of plastic hinges in beams. Although this effect does not significantly reduce the structural performance, addressing it could further improve the results.
- The inter-story drift ratios show a significant reduction and become much more uniform. The structure behaves more integrally, and sudden or irregular deformations are not observed.
- The unretrofitted model developed extensive nonlinear behavior in several beams and reached the LS–CP range before achieving the target displacement under the critical pushover loading pattern. This indicates that the original structure did not adequately satisfy the intended Life Safety performance objective.
- From a practical perspective, steel bracing can be an effective retrofit solution for improving the seismic response of the investigated RC building. Nevertheless, the increase in base shear may also increase demands on foundations, brace connections, collectors, and adjoining RC members; these components should therefore be checked in a complete retrofit design.
- The results of the present study are generally consistent with previous investigations showing that the addition of steel braces increases the lateral stiffness and strength of existing RC frames and reduces their displacement demands. However, the magnitude and distribution of the improvement depend strongly on the structural configuration, brace arrangement, and analysis direction. In contrast to studies focused mainly on regular buildings or steel frames, the present work examines a three-dimensional L-shaped RC building, in which the re-entrant corner and plan irregularity can amplify torsional response and produce non uniform drift concentrations. The results indicate that the bracing system reduces these concentrations and promotes a more uniform distribution of deformation over the building height. This provides a more specific contribution than studies that evaluate bracing only in regular planar frames.

9. Future Work Recommendations

To expand upon the findings of this study and address the inherent limitations of the current research, the following directions are recommended for future work:

- While this study utilized nonlinear static (pushover) analysis, future studies should perform Nonlinear Time History Analysis (NLTHA) using a suite of near-field and far-field ground motion records to capture the velocity-pulse and dynamic effects on the torsionally irregular L-shaped structure.
- Research should be conducted on optimization algorithms (e.g., genetic algorithms, particle swarm optimization) to determine the most effective spatial distribution and density of the steel bracing systems, targeting both cost minimization and performance maximization.

- A comparative study can be performed between the steel bracing system and other retrofitting techniques, such as Carbon Fiber Reinforced Polymer (CFRP) wrapping, RC shear walls, or modern passive energy dissipation devices like BRBs and dampers.
- The current model assumes a fixed-base condition. Future research should incorporate SSI to evaluate how different soil categories affect the seismic response, target displacement, and torsional coupling of irregular retrofitted structures.
- The study focused on plan irregularity (L-shape). Investigating the combined effects of vertical irregularities (such as setbacks or soft stories) and plan irregularities under bi-directional and tri-directional seismic excitations would provide a more comprehensive safety assessment.
- Developing analytical seismic fragility curves for before and after retrofitting cases would help quantify the reduction in collapse probability and assist in performance-based design and economic loss estimation.

Appendix

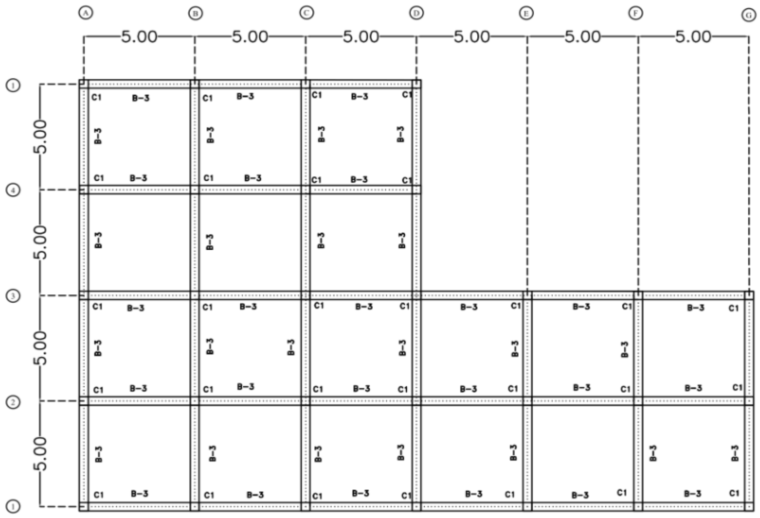

(a)

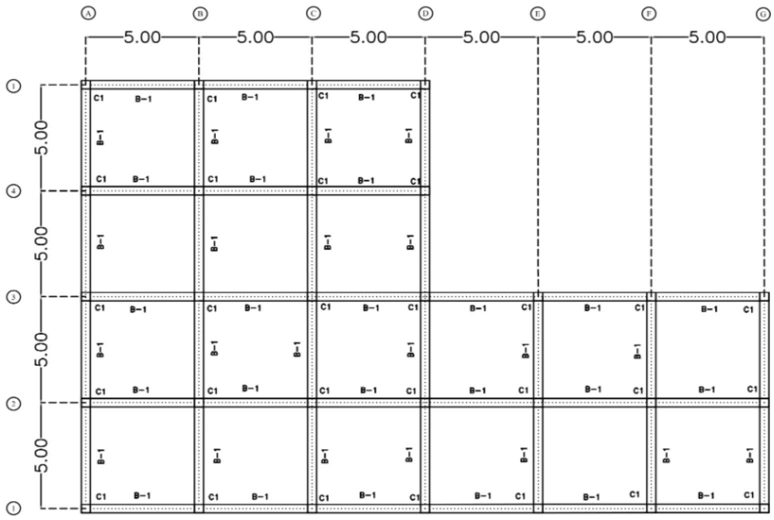

(b)

Fig. A. Framaing plan of the studied RC building. A) Story 1-6 B) Story 7-10

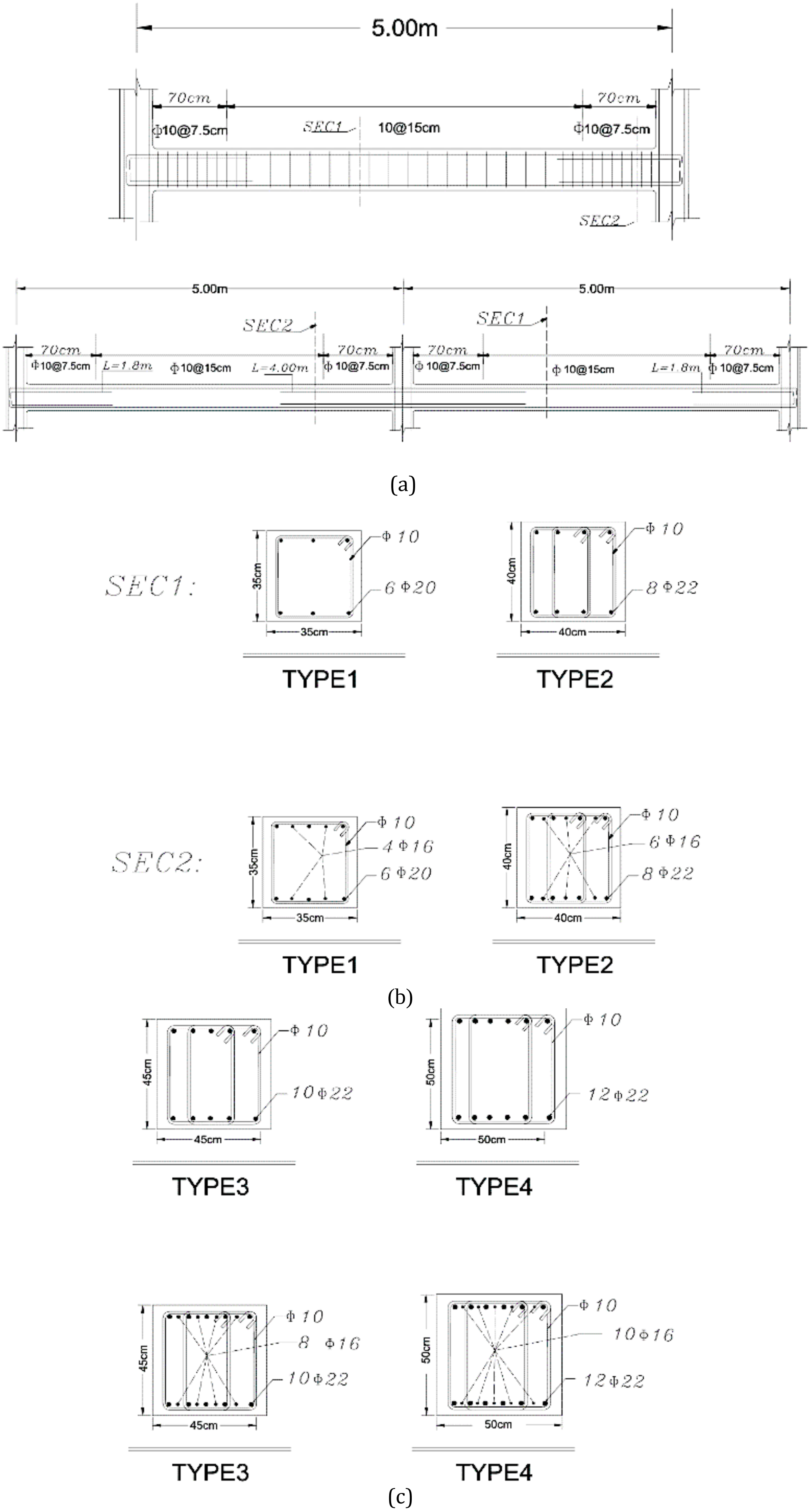

Fig. B. Details of RC beams of the studied building

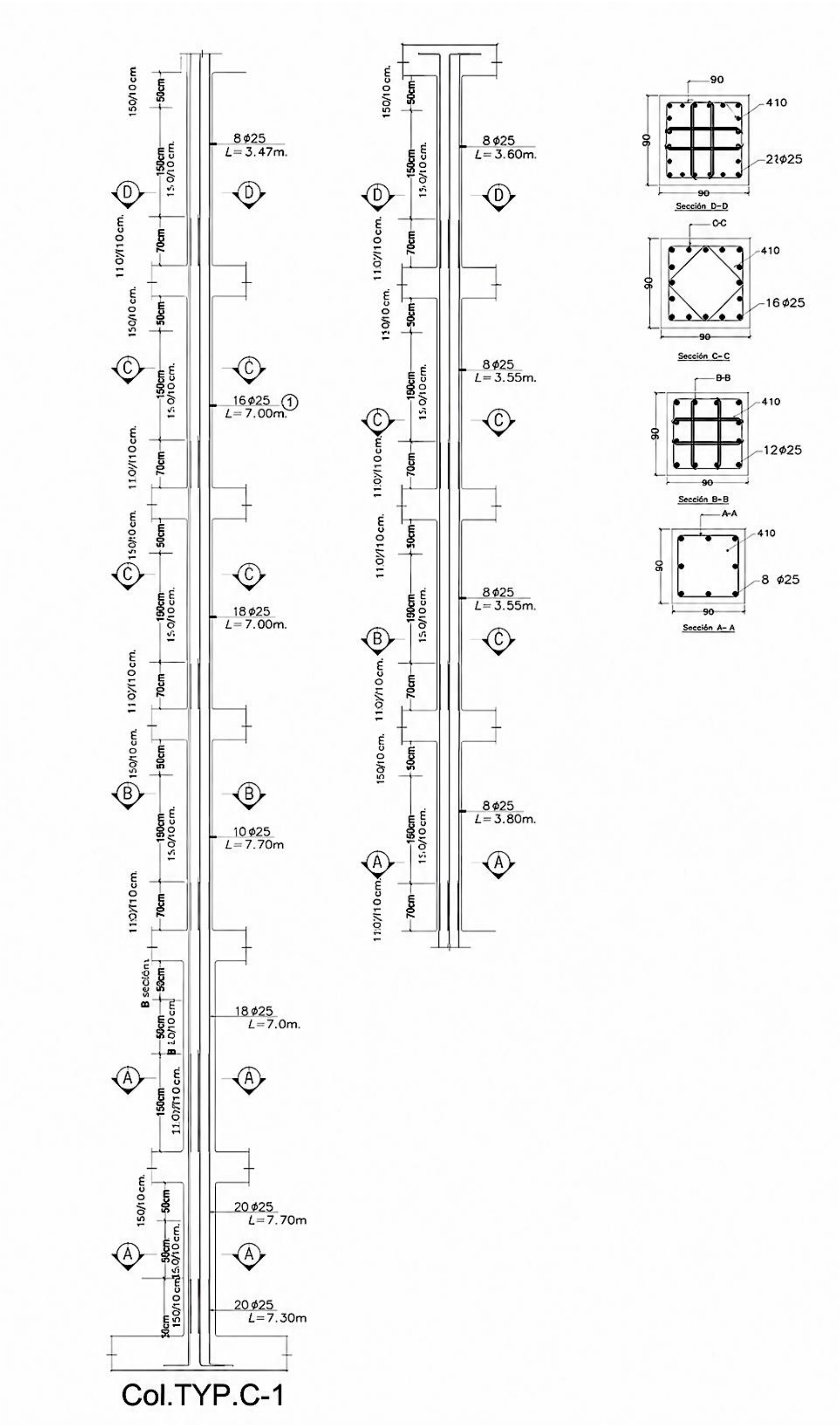

Fig. C. Details of RC columns of the studied building

References

[1] Pouraminian M, Hashemi S. V, Sadeghi A, Pourbakhshian S. Probabilistic Assessment the Seismic Collapse Capacity of Buckling-Restrained Braced Frames Equipped with Shape Memory Alloys. Journal of Structural and Construction Engineering 2021; 8(Special Issue 2), 129-149. (In Persian) https://doi.org/10.22065/jsce.2020.236804.2174.

[2] Marc B, O. JJ. Steel Bracing of RC Frames for Seismic Retrofitting. J Struct Eng 1990; 116:55–74. https://doi.org/10.1061/(ASCE)0733-9445(1990)116:1(55).

[3] Hu S, Liao Y, Zeng S, Sun Z, Peng X. Seismic retrofitting of existing reinforced concrete frames using eccentric steel braces: Experimental evaluation and numerical simulation. Structures 2026; 88:111824. https://doi.org/https://doi.org/10.1016/j.istruc.2026.111824.

[4] Hashemi S. V, Pouraminian M, Sadeghi A, Pourbakhshian S. Seismic Performance of Buckling Restrained Braced Frames with Shape Memory Alloy Subjected to Mainshock-Aftershock Near-Fault Ground Motion. Modares Civil Engineering Journal 2021; 21(4), 35-50. (In Persian)

[5] Khanal B, Chaulagain H. Seismic elastic performance of L-shaped building frames through plan irregularities. Structures 2020; 27:22–36. https://doi.org/10.1016/j.istruc.2020.05.017.

[6] Abdel Raheem SE, Ahmed MMM, Ahmed MM, Abdel-shafy AGA. Evaluation of plan configuration irregularity effects on seismic response demands of L-shaped MRF buildings. Bull Earthq Eng 2018; 16:3845–69. https://doi.org/10.1007/s10518-018-0319-7.

[7] Mazza F. Modelling and nonlinear static analysis of reinforced concrete framed buildings irregular in plan. Eng Struct 2014; 80:98–108. https://doi.org/10.1016/j.engstruct.2014.08.026.

[8] Vaziri SJ, Vahdani R, Souri O. Seismic evaluation of BRBF steel structures with L-shaped irregular plan considering soil structure interaction. Bull Earthq Eng 2024. https://doi.org/10.1007/s10518-024-01963-4.

[9] Vaziri SJ, Rajabnejad H, Soleymani A. Ground motion parameters and damage correlation in plan irregular L-shape steel structure with BRB. Soil Dyn Earthq Eng 2024; 186:108916. https://doi.org/10.1016/j.soildyn.2024.108916.

[10] Vaziri S Javad, Jarrahi Hossein, Asghari Nima. Effects of near-fault pulse-like and non-pulse-like seismic excitations on the structural response of steel high-rise buildings with buckling restrained braces. Adv Struct Eng 2025:13694332251399296. https://doi.org/10.1177/13694332251399295.

[11] Jaberi V, Vaziri SJ, Torabi L. A Practical and Innovative Alternative Framework for Plastic Design of Structures. Struct Des Tall Spec Build 2025; 34. https://doi.org/10.1002/tal.70062.

[12] Jarrahi H, Vaziri SJ, Khatibinia M. Sensitivity analysis and integrated optimization of placement and parameters of rotational friction dampers based on seismic energy approach considering soil-structure interaction. PLoS One 2025; 20:e0331741. https://doi.org/10.1371/journal.pone.0331741.

[13] Jarrahi H, Asadi A, Khatibinia M, Etedali S, Paknehad S. Soil-structure interaction effects on the seismic performance of steel moment-resisting frames equipped with optimal rotational friction dampers. Structures 2022; 43:449–64. https://doi.org/10.1016/j.istruc.2022.05.118.

[14] Jarrahi H, Asadi A, Khatibinia M, Etedali S, Samadi A. Simultaneous optimization of placement and parameters of rotational friction dampers for seismic-excited steel moment-resisting frames. Soil Dyn Earthq Eng 2020;136:106193. https://doi.org/10.1016/j.soildyn.2020.106193.

[15] Jarrahi H, Asadi A, Khatibinia M, Etedali S. Optimal design of rotational friction dampers for improving seismic performance of inelastic structures. J Build Eng 2020; 27:100960. https://doi.org/10.1016/j.jobe.2019.100960.

[16] Maheri MR, Fathi A. The Effects of X-Brace Configuration on the Seismic Performance of Retrofitted RC Frames. Iran J Sci Technol - Trans Civ Eng 2022; 46:3995–4018. https://doi.org/10.1007/s40996-022-00944-4.

[17] Rahimi A, Maheri MR. The effects of steel X-brace retrofitting of RC frames on the seismic performance of frames and their elements. Eng Struct 2020; 206. https://doi.org/10.1016/j.engstruct.2019.110149.

[18] Kheyroddin A, Sepahrad R, Saljoughian M, Ali M. Experimental evaluation of RC frames retrofitted by steel jacket , X - brace and X - brace having ductile ring as a structural fuse. J Build Pathol Rehabil 2019. https://doi.org/10.1007/s41024-019-0050-z.

[19] Tan H, Huang L, Yan L, Yi H. Seismic Behavior of Newly Constructed Three-Bay Steel X-Braced RC Space Frame 2014;8:1–17. https://doi.org/10.1142/S1793431114500122.

[20] Ahiwale DD, Penelope D, Darekar PL. Seismic performance assessment of reinforced concrete frames with different bracing systems. Innov Infrastruct Solut 2023;8:1–18. https://doi.org/10.1007/s41062-023-01071-3.

[21] Hodaipour Y, Ferdousi A. Analytical Investigation of the Effect of Steel X-Bracing Connection Type on the Reinforced Concrete Frames 2022;54:449–52. https://doi.org/10.22060/ceej.2021.19238.7129.

[22] Shoaib M, Abdul K, Ubaidullah B. Seismic upgrade of deficient RC frames using different configurations of eccentric steel braces. Asian J Civ Eng 2020. https://doi.org/10.1007/s42107-020-00325-0.

[23] Mazza F. Displacement-based seismic design of hysteretic damped braces for retrofitting in-plan irregular RC framed structures. Soil Dyn Earthq Eng 2014; 66:231–40. https://doi.org/10.1016/j.soildyn.2014.07.001.

[24] Mazza F. Nonlinear seismic analysis of unsymmetric-plan structures retrofitted by hysteretic damped braces. Bull Earthq Eng 2016; 14:1311–31. https://doi.org/10.1007/s10518-016-9873-z.

[25] Ferraioli M, Lavino A, Lauro G Di, Mandara A. Seismic Retrofit Of A Reinforced Concrete School Building Using Dissipative Steel Braces 2017:12–5.

[26] Saberi V, saberi H, Babanegar M, Sadeghi A, Moafi A. Investigation the Effect of Cutting the Lateral Bearing System and Very Soft Story Irregularities on the Seismic Performance of Concentric Braced Frames. Journal of Structural and Construction Engineering 2021; 8(Special Issue 3), 271-295. (In Persian). https://doi.org/10.22065/jsce.2021.243546.2215.

[27] Poudel S, Gyawali T.R. Structural performance of symmetric and asymmetric plan irregular building structures : A comparative analysis of conventional and grid slab systems Bull Earthquake Eng 2025; 23: 3395–420. https://doi.org/10.1007/s10518-025-02179-w.

[28] Chonratana Y, Chatpattananan V. A Damage Index for Assessing Seismic-Resistant Designs of Masonry Wall Buildings Reinforced with X-Bracing Concrete Frames. Applied Sciences 2023; 13(23):12566. https://doi.org/10.3390/app132312566

[29] ASCE/SEI 7-22. Minimum Design Loads and Associated Criteria for Buildings and Other Structures. Reston: American Society of Civil Engineers 2022.

[30] ASCE 41: American Society of Civil Engineers. Seismic Evaluation and Retrofit of Existing Buildings. Reston, VA: ASCE 2023.

[31] Prestandard F. commentary for the seismic rehabilitation of buildings (FEMA356). Washington, DC Fed Emerg Manag Agency 2000.

[32] Guideline for Seismic Rehabilitation of Existing Buildings. Tehran, Iran: Plan and Budget Organization 2013.

[33] Computers & Structures Inc. CSI Analysis Reference Manual for ETABS. ETABS Ref Man 2016.

[34] AISC 360: American Institute of Steel Construction. Specification for Structural Steel Buildings. Chicago, IL: AISC 2022.

[35] AISC 341: American Institute of Steel Construction. Seismic Provisions for Structural Steel Buildings. Chicago, IL: AISC 2022.

[36] ACI 318: American Concrete Institute. Building Code Requirements for Structural Concrete and Commentary. Farmington Hills, MI: ACI 2018.